Shpetner HS, Vallee RB (1989) Identification of dynamin, a novel mechanochemical enzyme that mediates interactions between microtubules. Cell 59:421–432

Strittmatter WJ, Weisgraber KH, Huang DY, Dong LM, Salvesen GS, Pericak-Vance M, Schmechel D, Saunders AM, Goldgaber D, Roses AD (1993) Binding of human apolipoprotein E to synthetic amyloid beta peptide: isoform-specific effects and implications for late-onset Alzheimer disease. Proc Natl Acad Sci USA 90:8098–8102

Suzuki DT, Grigliatti T, Williamson R (1971) Temperature-sensitive mutations in *Drosophila melanogaster*. VII. A mutation (para-ts) causing reversible adult paralysis. Proc Natl Acad Sci USA 68:890–893

Wenham PR, Price WH, Blandell G. (1991) Apolipoprotein E genotyping by one-stage PCR. Lancet 337:1158–1159

Wijsman EM, Daw EW, Yu CE, Payami H, Steinbart EJ, Nochlin D, Conlon EM, Bird TD, Schellenberg GD (2004) Evidence for a novel late-onset Alzheimer disease locus on chromosome 19p13.2. Am J Hum Genet 75:398–409

Yao PJ (2004) Synaptic frailty and clathrin-mediated synaptic vesicle trafficking in Alzheimer's disease. Trends Neurosci 27:24–29

Zuchner S, Noureddine M, Kennerson M, Verhoeven K, Claeyes K, De Jonghe P, Merory J, Oliveira SA, Speer MC, Stenger JE, Walizada G, Zhu D, Pericak-Vance MA, Nicholson G, Timmerman V, Vance JM (2005) Mutations in the pleckstrin homology domain of dynamin 2 cause dominant intermediate Charcot–Marie-Tooth disease. Nat Genet 37:289–294

THE JOURNAL OF BIOLOGICAL CHEMISTRY VOL. 283, NO. 24, pp. 16488–16496, June 13, 2008

Enzymatic Characteristics of I213T Mutant Presenilin-1/γ-Secretase in Cell Models and Knock-in Mouse Brains

FAMILIAL ALZHEIMER DISEASE-LINKED MUTATION IMPAIRS γ-SITE CLEAVAGE OF AMYLOID PRECURSOR PROTEIN C-TERMINAL FRAGMENT β[*][S]

Received for publication, February 19, 2008, and in revised form, April 21, 2008 Published, JBC Papers in Press, April 21, 2008, DOI 10.1074/jbc.M801279200

Masafumi Shimojo[‡§], Naruhiko Sahara[‡], Tatsuya Mizoroki[‡], Satoru Funamoto[¶], Maho Morishima-Kawashima[‖], Takashi Kudo[**], Masatoshi Takeda[**], Yasuo Ihara[¶], Hiroshi Ichinose[§], and Akihiko Takashima[‡1]

From the [‡]Laboratory for Alzheimer's Disease, RIKEN Brain Science Institute, Wako-shi, Saitama 351-0198, Japan, the [§]Department of Life Science, Tokyo Institute of Technology, Nagatuda, Yokohama 226-8501, Japan, the [¶]Faculty of Life and Medical Sciences, Doshisha University, Kyoto 619-0225, Japan, the [‖]Department of Molecular Neuropathology, Hokkaido University, Sapporo 060-0812, Japan, and the [**]Department of Neuropsychiatry, Osaka University Medical School, Osaka 565-0871, Japan

Presenilin (PS)/γ-secretase-mediated intramembranous proteolysis of amyloid precursor protein produces amyloid β (Aβ) peptides in which Aβ species of different lengths are generated through multiple cleavages at the γ-, ζ-, and ε-sites. An increased Aβ42/Aβ40 ratio is a common characteristic of most cases of familial Alzheimer disease (FAD)-linked PS mutations. However, the molecular mechanisms underlying amyloid precursor protein proteolysis leading to increased Aβ42/Aβ40 ratios still remain unclear. Here, we report our findings on the enzymatic analysis of γ-secretase derived from I213T mutant PS1-expressing PS1/PS2-deficient ($PS^{-/-}$) cells and from the brains of I213T mutant PS1 knock-in mice. Kinetics analyses revealed that the FAD mutation reduced *de novo* Aβ generation, suggesting that mutation impairs the total catalytic rate of γ-secretase. Analysis of each Aβ species revealed that the FAD mutation specifically reduced Aβ40 levels more drastically than Aβ42 levels, leading to an increased Aβ42/Aβ40 ratio. By contrast, the FAD mutation increased the generation of longer Aβ species such as Aβ43, Aβ45, and >Aβ46. These results were confirmed by analyses of γ-secretase derived from I213T knock-in mouse brains, in which the reduction of *de novo* Aβ generation was mutant allele dose-dependent. Our findings clearly indicate that the mechanism underlying the increased Aβ42/Aβ40 ratio observed in cases of FAD mutations is related to the differential inhibition of γ-site cleavage reactions, in which the reaction producing Aβ40 is subject to more inhibition than that producing Aβ42. Our results also provide novel insight into how enhancing the generation of longer Aβs may contribute to Alzheimer disease onset.

Amyloid β (Aβ)[2] is a hydrophobic peptide that pathologically deposits in the brains of Alzheimer disease (AD) patients. The significant neurotoxicity of oligomeric and/or fibrillar Aβ aggregates indicates that accumulation of Aβ is a central pathogenic event in AD (1). Sequential cleavage of β-amyloid precursor protein (APP) by β- and γ-secretases releases Aβ into the luminal/extracellular space. β-secretase is a membrane-bound aspartic protease (identified as BACE) that cleaves the extracellular region of APP to produce membrane-spanning APP C-terminal fragment β (termed CTFβ or C99) and a N-terminal secreted form of APPβ. The intramembranous region of CTFβ is cleaved next by γ-secretase to produce Aβ and APP intracellular domain, and because of the loose site specificity of γ-secretase-mediated proteolysis, various C-terminal truncated Aβ species, including two major species, Aβ40 and Aβ42, are also generated (1). Aβ40 is the most predominant species of secreted Aβ. Aβ42 is hypothesized to be the trigger species for AD-related amyloid pathophysiology, because it has much faster aggregation potential than Aβ40. Indeed, histochemical and biochemical studies have revealed that Aβ42 primarily deposits within the brains of AD patients and several animal models (2–4). Most importantly, mutations of APP, presenilin-1 (PS1), and PS2 have been identified in familial Alzheimer disease (FAD) and have been found to specifically increase the Aβ42/Aβ40 ratio in cell medium or animal tissues and to accelerate the parenchymal accumulation of Aβ (5–9). In this way, γ-secretase-mediated Aβ metabolism may be critically involved in the onset of AD.

Accumulating evidence strongly indicates that γ-secretase is a high molecular weight membrane protein complex in which PS serves as a catalytic subunit (10). PS proteins are hydrophobic multiple membrane-spanning proteins that become activated through endoproteolysis of its large cytosolic loop domain, producing N- and C-terminal fragments (11–14). The

* The costs of publication of this article were defrayed in part by the payment of page charges. This article must therefore be hereby marked "*advertisement*" in accordance with 18 U.S.C. Section 1734 solely to indicate this fact.

[S] The on-line version of this article (available at http://www.jbc.org) contains supplemental Fig. 1.

[1] To whom correspondence should be addressed: 2-1 Hirosawa, Wako-Shi, Saitama 351-0198, Japan. Tel.: 81-48-467-9704; Fax: 81-48-467-5916; E-mail: kenneth@brain.riken.jp.

[2] The abbreviations used are: Aβ, amyloid β; PS, presenilin; APP, amyloid precursor protein; AD, Alzheimer disease; FAD, familial AD; WT, wild-type; CTFβ, C-terminal fragment β; CHAPSO, 3-[(3-cholamidopropyl)dimethylammonio]-2-hydroxy-1-propanesulfonic acid; MEF, mouse embryonic fibroblast; PIPES, 1,4-piperazinediethanesulfonic acid; TLCK, 1-chloro-3-tosylamido-7-amino-2-heptanone; Tricine, *N*-[2-hydroxy-1,1-bis(hydroxymethyl)ethyl]glycine.

N- and C-terminal fragments incorporate into the stable high molecular weight complex, which consists of at least three minimum cofactors: nicastrin, APH-1, and PEN-2 (11–13). Two conserved aspartate (Asp^{257} and Asp^{385} in PS1) residues, which are located within transmembrane domains 6 and 7, form the predicted active center of the PS/γ-secretase complex (10). Various type I membrane protein substrates, including APP and Notch, undergo regulated intramembranous proteolysis within the hydrophobic lipid bilayer environment (14, 15).

On the basis of this model, we hypothesize that the mechanisms underlying the increased Aβ42/Aβ40 ratio observed in cases of FAD-linked PS mutations might directly reflect an alteration of the enzymatic characteristics of the PS/γ-secretase complex. More than 150 FAD-linked mutations have been identified in PS genes (1). These widely distribute to every sequence of PS proteins, indicating that each mutation can potentially modify the catalytic reactions of γ-secretase enzyme in a distinct manner. Numerous cell culture studies have revealed various aspects of PS mutations and their effects; nevertheless, experimental differences, such as the variations in cell models, detection systems, and normalization methodology, among individual studies make the study of PS mutations through living cell-based methods a controversial issue (16, 17). Traditionally, γ-secretase was believed to mainly hydrolyze the covalent bonds at Val^{40}–Ile^{41} and Ala^{42}–Thr^{43} of CTFβ (termed γ-sites), generating Aβ40 and Aβ42, respectively (1). The γ-sites were thus regarded as the major cleavage sites targeted by γ-secretase. However, recent studies have revealed novel cleavage sites: γ-secretase also mediates the cleavage of ζ- and ϵ-sites, which are closer to the cytoplasmic membrane boundary (18–20). Cleavage at the ζ- and ϵ-sites produces various longer Aβ (>Aβ43) species, and evidence indicates that these species may be processed to shorter Aβ species in stages (21, 22). Taken together, these findings suggest that γ-secretase-mediated proteolysis consists of multiple complicated cleavage reactions that relate to each other along the transmembrane domain of APP-CTFβ. Nonetheless, it is still unclear how FAD mutations modify overall γ-secretase-mediated cleavage of APP, leading to increased Aβ42/Aβ40 ratios. The molecular mechanisms underlying this process also remain elusive. This crucial issue requires more careful assessment from the aspect of the enzymatic characteristics of the PS/γ-secretase complex.

These findings prompted us to evaluate the activity kinetics of the wild-type (WT) and FAD mutant PS1/γ-secretase enzyme by using a CHAPSO solubilization γ-secretase assay system (23, 24). This strategy has great advantages because it enables us not only to directly assess the effect of mutations on the enzyme in cell models but also in brain tissues, which should better reflect the physiological status of the enzyme *in vivo*. We previously generated PS1/PS2-deficient cell lines that stably express either the WT or FAD mutant forms of human PS1 (25). Consistent with previous reports (8, 9), we demonstrated that FAD mutations reduced the secretion of Aβ peptides (25). Thus, one possible mechanism underlying increased Aβ42/Aβ40 ratios is that FAD mutations might directly impair the enzymatic activity of γ-secretase, thereby modifying the individual cleavage reactions that produce Aβ40 and Aβ42. In this study, we specifically focused on the effect of the I213T FAD-linked PS1 mutation on γ-secretase and reported the enzymatic characteristics of γ-secretase derived both from cell models and from the brains of knock-in mice.

EXPERIMENTAL PROCEDURES

Antibodies—Anti-PS1 N-terminal mouse monoclonal antibody (AD3.4, 1:1,000) and anti-PS1 C-terminal rabbit polyclonal antibody (AD3C, 1:1,000) were described previously (25). Rabbit polyclonal antibodies against the C-terminal sequences of APH-1aL (ACS-01, 1:1,000) and PEN-2 (PCS-01, 1:1,000) were generated previously (25). Mouse monoclonal antibody against the N-terminal region of nicastrin was purchased from Chemicon. End-specific antibodies against Aβ N-terminal (82E1, 1:100); Aβ40 (1A10, 1:50); and Aβ42 C-terminal (1:50) were purchased from IBL.

Plasmid DNA Constructs and Cell Cultures—$PS^{+/+}$ and PS1/PS2-deficient ($PS^{-/-}$) mouse embryonic fibroblast (MEF) cells (kindly provided by Dr. B. De Strooper, K. U. Leuven and Flanders Interuniversitary Institute for Biotechnology, Belgium) (26, 27) were cultured in Dulbecco's modified Eagle's medium supplemented with 10% fetal bovine serum and 100 μg/ml gentamicin at 37 °C in a 5% CO_2 incubator. $PS^{-/-}$ MEF-based cell lines stably expressing either WT or I213T FAD mutant human PS1 were described previously (25). To establish cell lines that stably express dominant negative mutant D257A human PS1, we generated cDNA by using a conventional two-step PCR protocol and a primer pair for D257A (5′-ATT TCA GTA TAT GCT TTA GTG GCT GTT-3′ and 5′-AAC AGC CAC TAA AGC ATA TAC TGA AAT-3′). The cDNA was then subcloned into the EcoRI/XhaI site of a pCI-Bls vector; the DNA sequence was confirmed with an ABI DNA sequencer. After transfection into $PS^{-/-}$ MEF cells, several clonal lines were selected in 7.5 μg/ml blasticidin S. All stable cell lines were maintained in growth medium containing 5.0 μg/ml blasticidin S.

I213T Knock-in Mice—We genotyped 11.0–12.5-month-old homozygous (I213T/I213T, $n = 4$), hemizygous (+/I213T, $n = 9$), and control (+/+, $n = 5$) I213T mutant PS1 knock-in mice for WT and mutant alleles by PCR, as described previously (28, 29). Fresh whole brains were immediately dissected and used for further biochemical preparations and enzyme assays. All procedures involving animals and their care were approved by the Animal Care Use Committee of the RIKEN Brain Science Institute.

Preparation of Solubilized γ-Secretase and Recombinant APP-C99-FLAG Substrate—Semi-confluent cultured cells (60 × 100-mm dish) were washed with phosphate-buffered saline and disrupted in homogenization buffer (20 mM HEPES-NaOH, pH 7.4, 150 mM NaCl, 10% (v/v) glycerol, 5 μg/ml antipain, 5 μg/ml leupeptin, 2 μg/ml aprotinin, and 0.5 mM pH blocker) using a Teflon homogenizer (1,200 rpm, 20 strokes). After removal of nuclei and cell debris through two centrifugations (1,500 × *g*, 4 °C, 10 min), the post-nuclear supernatant was ultracentrifuged (100,000 × *g*, 4 °C, 1 h). The precipitate was washed with homogenization buffer, ultracentrifuged (100,000 × *g*, 4 °C, 1 h), and finally collected as crude microsomal membranes. These membranes were then resuspended

with resuspension buffer (50 mM PIPES-NaOH, pH 7.0, 250 mM sucrose, and 1 mM EGTA), and the amount of protein was quantitated with a BCA kit (Pierce). Protein was adjusted to a final concentration of 10 mg/ml. To prepare enzyme fractions, we added equal amounts of 2× NK buffer (50 mM PIPES-NaOH, pH 7.0, 250 mM sucrose, 1 mM EGTA, 2% (w/v) CHAPSO, 10 μg/ml antipain, 10 μg/ml leupeptin, 10 μg/ml aprotinin, 1 mM pH blocker, 20 μg/ml TLCK, 10 mM 1.10-phenanthroline, and 2 mM thiorphan) to the membrane suspension and incubated the mixture for 1 h on ice. After ultracentrifugation (100,000 × *g*, 4 °C, 1 h), the supernatant containing solubilized γ-secretase was collected and stored at −80 °C.

Baculovirally expressed recombinant C99-FLAG substrate was prepared as described previously (24). Briefly, lysates from C99-FLAG-overexpressing Sf9 cells were extracted in lysis buffer (50 mM Tris-HCl, pH 7.4, 150 mM NaCl, 5 mM EDTA, and 1% (v/v) Nonidet P-40) containing a protease inhibitor mixture (Roche Diagnostics) on ice for 1 h. After ultracentrifugation (245,000 × *g*, 20 min), solubilized C99-FLAG was agitated with anti-FLAG M2-agarose beads (Sigma) overnight. After sequential washing of the beads with 50-fold bed volumes of 0.5% Nonidet P-40 in lysis buffer, bound C99-FLAG was eluted by adding 100 mM glycine HCl (pH 2.7). Eluted C99-FLAG was immediately neutralized with 1 M Tris base. The resulting solution was further concentrated with a Centricon YM-3 (3,000 MWCO) and then stored at −80 °C until use.

In Vitro CHAPSO-solubilized γ-Secretase Assay—*In vitro* γ-secretase-mediated *de novo* Aβ generation was measured by using a method described previously (24). Briefly, 1% CHAPSO-solubilized γ-secretase was mixed with 3 volumes of CHAPSO-free assay buffer (50 mM PIPES-NaOH, pH 7.0, 250 mM sucrose, 1 mM EGTA, 5 μg/ml antipain, 5 μg/ml leupeptin, 5 μg/ml aprotinin, 500 μM pH blocker, 10 μg/ml TLCK, 5 mM 1.10-phenanthroline, 1 mM thiorphan, and 0.133% (w/v) phosphatidylcholine) and incubated with 0.1–2.5 μM recombinant C99-FLAG substrate at 37 °C. As previous studies mentioned, 0.1% phosphatidylcholine enhances the basal levels of Aβ generation without affecting the Aβ42/Aβ40 ratio (24, 30). The final concentration of C99-FLAG stock solution containing Nonidet P-40 in the reactions was roughly estimated to be <0.07%, a concentration that does not noticeably affect *de novo* Aβ production. To quantitate *de novo* generated Aβs, samples were collected at different time points and excess lipids in the assay mixture were removed by adding $CHCl_3$:MeOH (2:1) and $CHCl_3$:MeOH:MilliQ (1:2:0.8). After drying, sample pellets were re-dissolved in 1× Sample buffer and then subjected to SDS-PAGE/immunoblot analysis with Aβ N- or C-terminal end-specific antibodies. To detect various longer Aβ species, Aβ1–37 through Aβ1–46 were separated by SDS-PAGE and 8 M urea-containing modified Tris-Tricine gels, and 82E1 antibody was used as a probe (21). All quantitated data were calculated by comparing chemiluminescence signal intensities of Aβ species to synthetic Aβ1–40 or Aβ1–42 standard calibration curves (AnaSpec or Peptide Inc.). Inhibition analyses were performed with two γ-secretase-specific inhibitors, DAPT and WPE-III-31C, purchased from Calbiochem (final dimethyl sulfoxide concentration was <1.0% (v/v)).

Calculation of Kinetics Constants—Michaelis-Menten kinetics constants (V_{max} and K_m) were calculated by fitting experimental data to Lineweaver-Burk plots according to the equation $1/[V] = K_m/V_{max}[S] + 1/V_{max}$, where $[V]$ is the reaction velocity of Aβ generation, and $[S]$ is the concentration of the APP-C99-FLAG substrate. To calculate the values of V_{max} and K_m, experimentally measured values of $[V]$ determined from experiments using a range of high C99-FLAG concentrations were used for linear fitting because $[V]$ measured from experiments using low C99-FLAG concentrations contains a large experimental error, which interferes with appropriate linear fitting.

Statistical Analysis—Statistical significance of data were tested with a Student's *t* test or a Tukey-Kramer test. Data were analyzed with InStat version 3.0a (GraphPad).

RESULTS

Enzymatic Characteristics of Wild-type PS1/γ-Secretase in PS$^{-/-}$ MEF Cell Models—To characterize γ-secretase activity using a CHAPSO-solubilized assay system, first we solubilized purified crude microsomal membranes from PS$^{+/+}$ MEF, PS$^{-/-}$ MEF, and WT line 38 (WT38) cells, which stably express endogenous levels of WT human PS1 on a PS$^{-/-}$ MEF background, and incubated these membranes with 500 nM C99-FLAG. Immunoblotting with anti-Aβ N- and C-terminal end-specific antibodies showed that PS$^{+/+}$ MEF lysates displayed robust amounts of *de novo* Aβ generation, including Aβ40 and Aβ42 generation after 4 h of incubation (Fig. 1, *A* and *B*). Relatively higher Aβ42/Aβ40 ratios (about 40–50%) compared with secreted Aβ ratios were observed in this assay system (25). By contrast, immunoblotting of PS$^{-/-}$ MEF lysates failed to detect any Aβ, even after 4 h of incubation, thus completely excluding possible PS-independent nonspecific *de novo* Aβ generation activity due to contaminating proteases. As expected, expression of WT human PS1 significantly restored *de novo* Aβ generation activity to levels similar to those detected in PS$^{+/+}$ MEF lysates (Fig. 1, *A* and *B*). We observed a slightly lower Aβ42/Aβ40 ratio in reaction mixtures containing WT38 lysates compared with those containing PS$^{+/+}$ MEF lysates. This difference might reflect the absence of PS2 or differences between mouse and human PS1 species.

To examine the reaction kinetics of *in vitro* γ-secretase, next we monitored the time course of Aβ generation. The levels of each Aβ species increased in a linear fashion for up to 5 h, indicating that the initial velocity of the enzyme-substrate reaction was stable during this period (data not shown). The rate of Aβ generation fit to a Michaelis-Menten-like reaction curve (Fig. 1*C*). V_{max} values for PS$^{+/+}$ MEF and WT38 lysates were 790.60 ± 37.01 pM/min and 686.80 ± 198.73 pM/min, respectively, and K_m values were 2.08 ± 0.13 μM and 2.26 ± 1.40 μM, respectively (Fig. 1*C*). These results approximately corresponded to those of previous studies (23, 24, 31) and suggest that the enzymatic characteristics of γ-secretase in both types of cell lysates are not much different. The V_{max} and K_m values of Aβ40 for PS$^{+/+}$ MEF lysates were 150.99 ± 33.77 pM/min and 0.90 ± 0.30 μM, respectively, and the V_{max} and K_m values of Aβ40 for WT38 were 124.27 ± 12.68 pM/min and 0.70 ± 0.07 nM, respectively. However, we could not estimate the V_{max} and

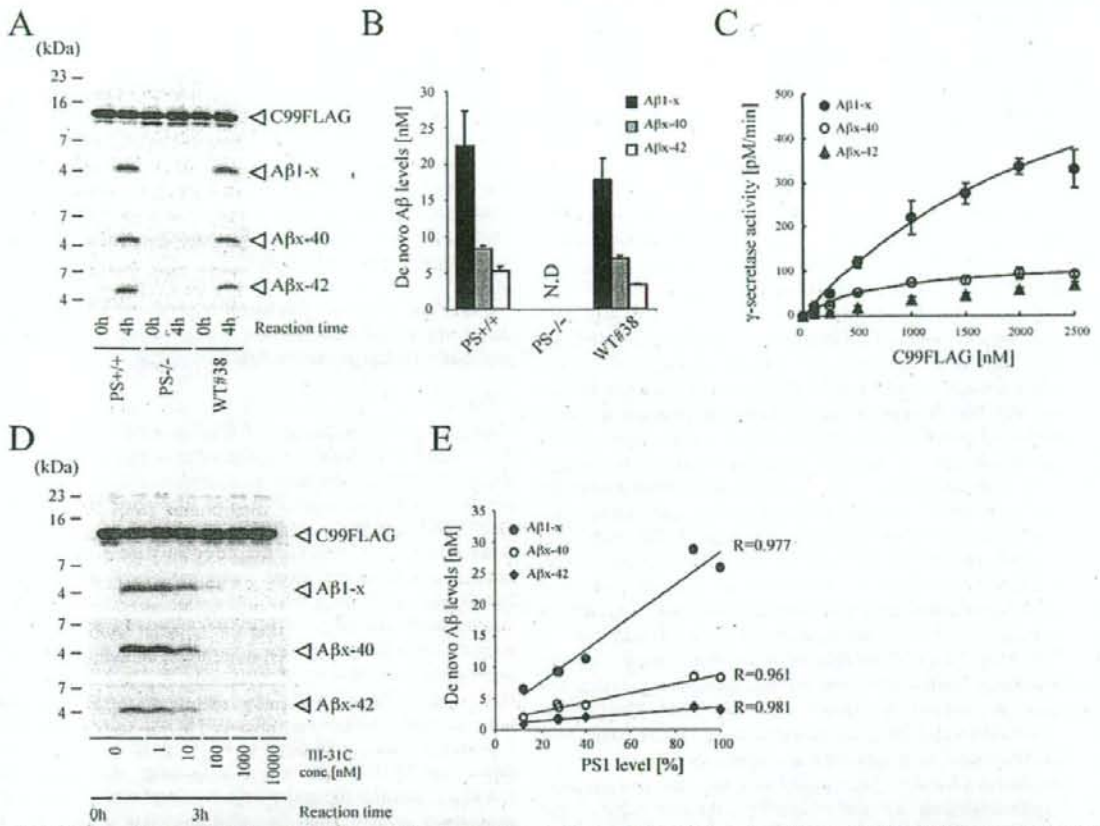

FIGURE 1. **Enzymatic characteristics of CHAPSO-solubilized γ-secretase.** *A*, after incubation of lysates with 500 nM C99-FLAG at 37 °C for 0 or 4 h, *de novo* generated Aβs were separated on 10/16.5% Tris-Tricine gels, which were then immunoblotted with anti-Aβ N- or C-terminal-specific antibodies. *B*, the amounts of each Aβ species were estimated by comparing the densities of immunoreactive bands with those of standard synthetic Aβ1–40 and Aβ1–42 plotted on a calibration curve. Mean values ± S.D. of triplicate experiments are shown. *N.D.*, not determined. *C*, WT (line 38) lysates were incubated with the indicated concentrations of C99-FLAG at 37 °C for 4 h. The rate of *de novo* generation of each Aβ species followed a Michaelis-Menten-like reaction curve. Mean values ± S.D. from three independent experiments are shown. Theoretical reaction curves were fitted after K_m and V_{max} values were calculated. *D*, WT (line 38) lysates and 500 nM C99-FLAG were coincubated with the indicated concentrations of the γ-secretase inhibitor WPE-III-31C at 37 °C for 3 h. *E*, correlations between PS1 levels and *de novo* levels of each Aβ species are shown. CHAPSO-solubilized membrane fractions were prepared from six independent cell lines expressing various levels of WT PS1 (supplemental Fig. 1). After incubation with 500 nM C99-FLAG at 37 °C for 4 h, *de novo* Aβ species were measured. The relative level of PS1 in WT (line 38) lysate was set as 100% in the value of the *x* axis. *Dots* represent the mean values of triplicate analysis using each lysate.

K_m of Aβ42 because *de novo* Aβ42 levels continuously increased with increasing concentrations of C99-FLAG, resulting in a linear fit to the Lineweaver-Burk plot, which did not provide us with appropriate intercept values of the 1/[*V*] axis and 1/[S] axis. This difference in kinetics suggests the possibility that Aβ40 and Aβ42 are generated from distinct reactions. As recent studies have mentioned, the Aβ42/Aβ40 ratio gradually increases with increasing C99-FLAG concentrations (24, 32).

Accumulating evidence strongly indicates that PS itself works as the catalytic subunit of the γ-secretase complex. We confirmed this premise by demonstrating that expression of dominant negative human D257A mutant PS1 failed to restore *de novo* Aβ synthesis in $PS^{-/-}$ MEF cells and that 1% Triton X-100 solubilization, which disrupts the interaction of PS complex components, completely abolished Aβ generation (data not shown). The γ-secretase-specific inhibitors DAPT (data not shown) and WPE-III-31C (Fig. 1*D*) significantly suppressed the generation of each Aβ species in a dose-dependent manner at IC_{50} values of ~100 nM DAPT and ~10 nM WPE-III-31C. To evaluate expression levels of PS1 and *de novo* generation level of Aβ, we analyzed six independent stable cell lines, including the WT38 line (supplemental Fig. 1) (25). After incubation of the membrane fractions with 500 nM C99-FLAG, a linear correlation between PS1 levels and Aβ levels was observed (Fig. 1*E*), even though the Aβ42/Aβ40 ratio remained unchanged among these cell lines (supplemental Fig. 1*C*). Taken together, these results indicate that this assay system reflects exactly genuine PS-dependent γ-secretase activity. Thus, in all of the following experiments, we regarded PS1 protein levels as a relative unit of active enzyme.

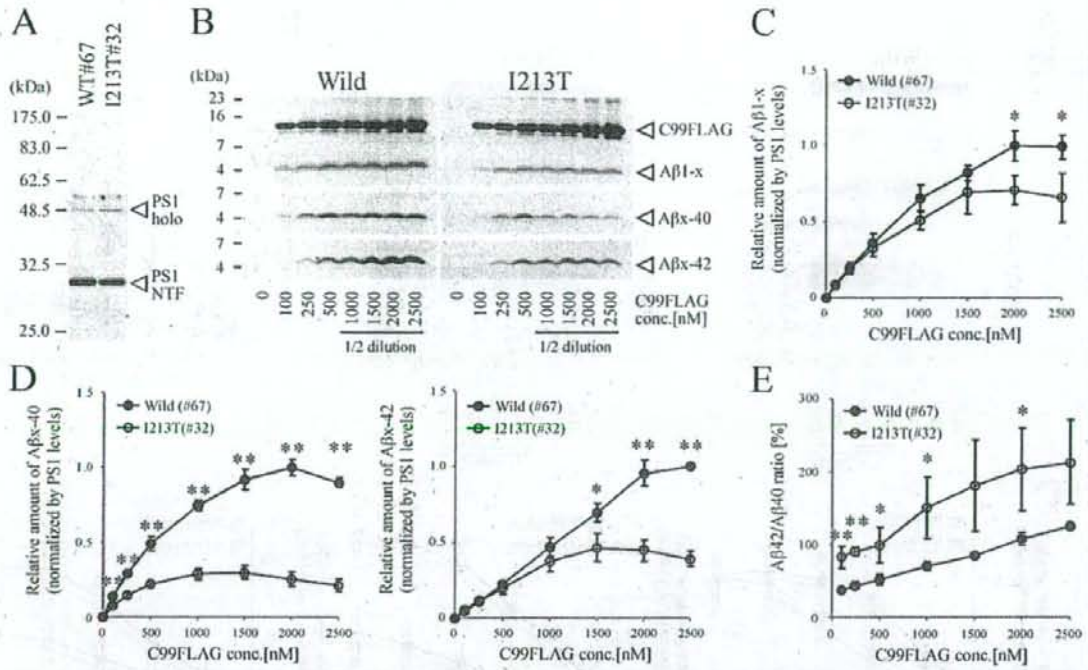

FIGURE 2. **FAD-linked PS1 mutations directly impair the catalytic activity of γ-secretase-mediated γ-site cleavage.** *A*, PS1 levels and expression profiles in CHAPSO-solubilized lysates from WT (line 67) or I213T (line 32) FAD mutant cells were analyzed by immunoblotting using anti-PS1 N terminus antibody. *NTF*, N-terminal fragment. *holo*, full-length PS1. *B*, CHAPSO-solubilized lysates from WT (line 67) or I213T (line 32) cells were individually coincubated with the indicated concentrations (*conc.*) of C99-FLAG at 37 °C for 4 h. Aβ, Aβ40, and Aβ42 in the reaction mixtures were separated in 10/16.5% Tris-Tricine gels, which were immunoblotted with anti-Aβ N- or C-terminal-specific antibodies. Typical immunoblot results of three independent experiments are shown. Note, for samples incubated with C99-FLAG concentrations of 1–2.5 μM, only one-half of the samples were loaded into the gels. *C*, comparative kinetics profiles of Aβ1-x generation per molecule of γ-secretase are shown. Relative amounts of Aβ were evaluated after normalization with PS1 protein levels. The value of WT enzyme with the maximum point was set to equal 1. *D*, comparative kinetics profiles of Aβx-40 and Aβx-42 generation per molecule of γ-secretase are shown. Both Aβ40 and Aβ42 levels were differentially attenuated by the I213T mutation. Relative amounts of Aβ were evaluated after normalization with PS1 protein levels. The value of WT enzyme with the maximum point was set to equal 1. *E*, the Aβ42/Aβ40 ratio increased in samples containing the mutant enzyme. *Dots* and *error bars* represent mean values ± S.D. from three individual experiments. The statistical significance of the data was tested with a Student's *t* test. *, $p < 0.05$; **, $p < 0.01$.

I213T FAD-linked Mutations Partially Impair γ-Secretase-mediated γ-Site Cleavage—In our previous study, we reported that expression of FAD mutant PS1 in $PS^{-/-}$ MEF cells failed to restore the ability of these cells to secrete Aβ peptides, leading us to propose that FAD mutations might attenuate γ-site cleavage reactions by directly modifying the enzyme characteristics of γ-secretase (25). To test this hypothesis, we assessed the rate that PS1/γ-secretase generated Aβs in cells expressing either WT PS1 or I213T FAD mutant PS1. WT and I213T FAD mutant cell lysates were coincubated with C99-FLAG at 0–2.5 μM concentrations, and the rate of Aβ generation was measured. Cell lines expressing similar levels of each PS1 variant were chosen in order to minimize experimental error (Fig. 2*A*), and the relative amounts of Aβ per molecule of WT and I213T FAD mutant PS1/γ-secretase were evaluated after normalization with PS1 protein levels. As shown in Fig. 2*B*, the I213T mutation moderately attenuated the rate of Aβ generation compared with that of WT. Suppression was specific and significant at high concentrations (2.0–2.5 μM) of C99-FLAG substrate. Moreover, V_{max} of Aβ generation also tended to decrease by 30% (Fig. 2, *B* and *C*). This suggests that the I213T mutation directly and specifically impaired γ-secretase enzymatic activity responsible for overall Aβ generation.

We further examined the generation rate of both Aβ40 and Aβ42 species. As expected, the I213T mutation drastically attenuated Aβ40 levels compared with WT levels (Fig. 2, *B* and *D*) by about 80% at the maximum concentration of C99-FLAG. Although the I213T mutation attenuated Aβ42 levels at C99-FLAG concentrations of 1.5–2.5 μM (Fig. 2, *B* and *D*), levels observed at 0.1–1.0 μM C99-FLAG were comparable with those measured from cells expressing the WT enzyme. The reduction of Aβ40 levels was more drastic than that of Aβ42, indicating that the I213T mutation certainly increases the Aβ42/Aβ40 ratio (Fig. 2*E*). Taken together, these results indicate that the I213T mutation impairs γ-site cleavage reactions affecting both Aβ40 and Aβ42 generation and that differential efficiency in reducing Aβ40 and Aβ42 ultimately results in a higher Aβ42/Aβ40 ratio.

I213T Mutant PS1 Enzyme Facilitates the Generation of Longer Aβ Species—Recent studies have identified various longer Aβ species (>Aβ43) generated from γ-secretase-mediated ζ- and ε-site cleavage (21, 33). The results shown in Fig. 2 demon-

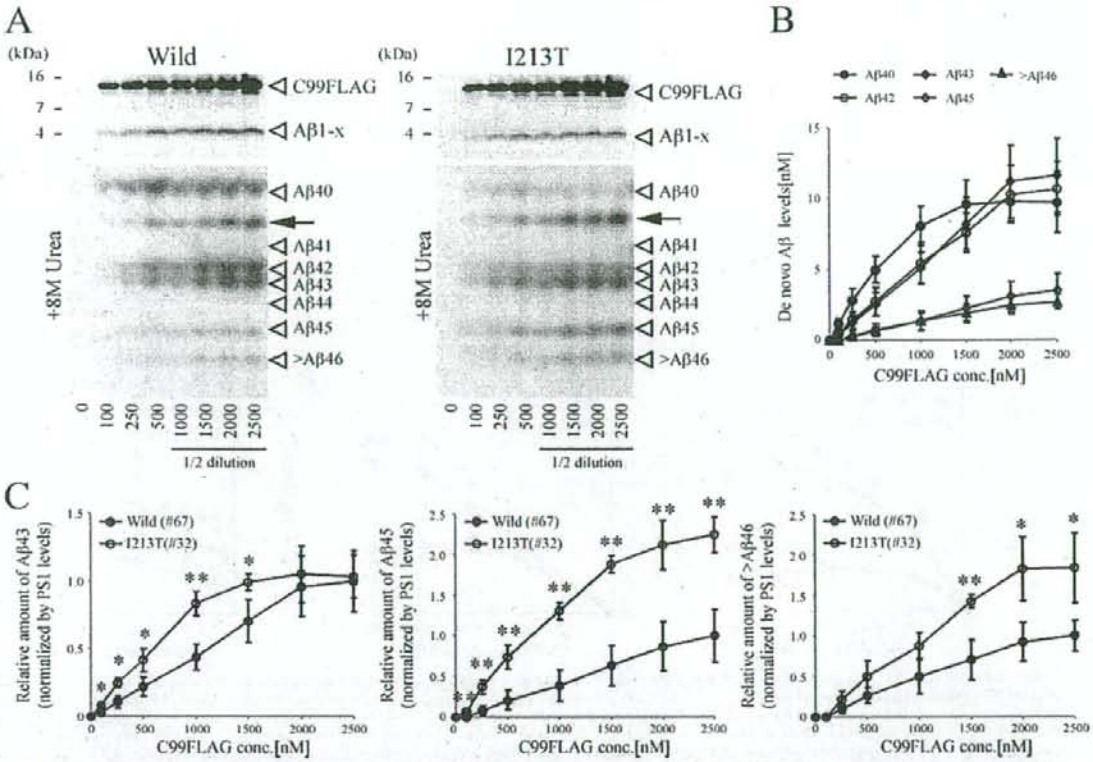

FIGURE 3. **FAD-linked PS1 mutations facilitate the generation of longer Aβ species.** *A*, longer Aβ species were separated by SDS-PAGE on 8 M urea-containing modified Tris-Tricine gels, which were then blotted and probed with 82E1 antibody. Typical immunoblotting results of three independent experiments are shown. Note that for samples incubated with C99-FLAG concentrations, only one-half of the samples were loaded into the gels. The *arrow* indicates carboxyl-truncated C99-FLAG fragments (24). *B*, Michaelis-Menten-like reaction curves for each Aβ species identified in samples containing WT (line 67) enzyme are shown. *conc.*, concentration. *Dots* and *error bars* represent mean values ± S.D. from three individual experiments. *C*, comparative kinetics profiles of Aβ43, Aβ45, and >Aβ46 generation per molecule of γ-secretase are shown. *Dots* and *error bars* represent mean values ± S.D. from three individual experiments. Relative amounts of Aβ were evaluated after normalization with PS1 protein levels. The value of WT enzyme with the maximum point was set to equal 1. The statistical significance of the data was tested with a Student's *t* test. *, $p < 0.05$; **, $p < 0.01$.

strate that the I213T mutation clearly impairs the production of Aβ40 and Aβ42, affecting the rate at which these Aβs are generated. Nevertheless, the overall levels of Aβ produced were not greatly affected by the I213T mutation. This suggests that the mutant enzyme may facilitate the generation of longer Aβ species. To address this possibility, we measured the levels of each Aβ species in the reaction mixtures by SDS-PAGE of 8 M urea-containing modified Tris-Tricine gels, which enabled us to separate various long Aβ species by the lengths of their C-terminal amino acid residues (21). We successfully observed PS-dependent *de novo* generation of not only Aβ40 and Aβ42 but also of Aβ43, Aβ45, and >Aβ46 species in samples from WT PS1/γ-secretase-expressing cells (Fig. 3, *A* and *B*). The levels of each Aβ species increased in a linear, time-dependent fashion, and the γ-secretase inhibitors (DAPT and WPE-III-31C) clearly suppressed this increase in a dose-dependent manner (data not shown). Next, we compared the levels of each Aβ species in cells expressing I213T FAD mutant PS1/γ-secretase to those in cells expressing WT PS1/γ-secretase. Interestingly, the I213T mutation increased the generation rate of longer forms of Aβs, including Aβ43, Aβ45, and >Aβ46 species, compared with WT (Fig. 3, *A* and *C*). Aβ43 levels were significantly enhanced at C99-FLAG substrate concentrations of 0.1–1.5 μM, plateauing at higher concentrations. In contrast, >Aβ46 levels were strongly enhanced at C99-FLAG concentrations of 1.5–2.5 μM. Unlike Aβ43 and >Aβ46 levels, Aβ45 levels remained enhanced regardless of the C99-FLAG concentration. These results indicate that the I213T mutation facilitates the production of longer Aβ species as opposed to inhibiting the production of shorter Aβ species. These results also suggest that a highly related mechanism may exist that links the generation of Aβ species of different lengths.

γ-Secretase Activity in I213T Mutant PS1 Knock-in Mouse Brain—To extend the findings obtained from cell models and to examine the physiological status of γ-secretase activity *in vivo*, we assessed γ-secretase activity in samples purified from I213T PS1 knock-in mouse brain. The protein levels of PS1 and of other γ-secretase complex components in CHAPSO-solubilized microsomal fractions were not significantly different among mice of each genotype (Fig. 4*A*). Thus, with this model,

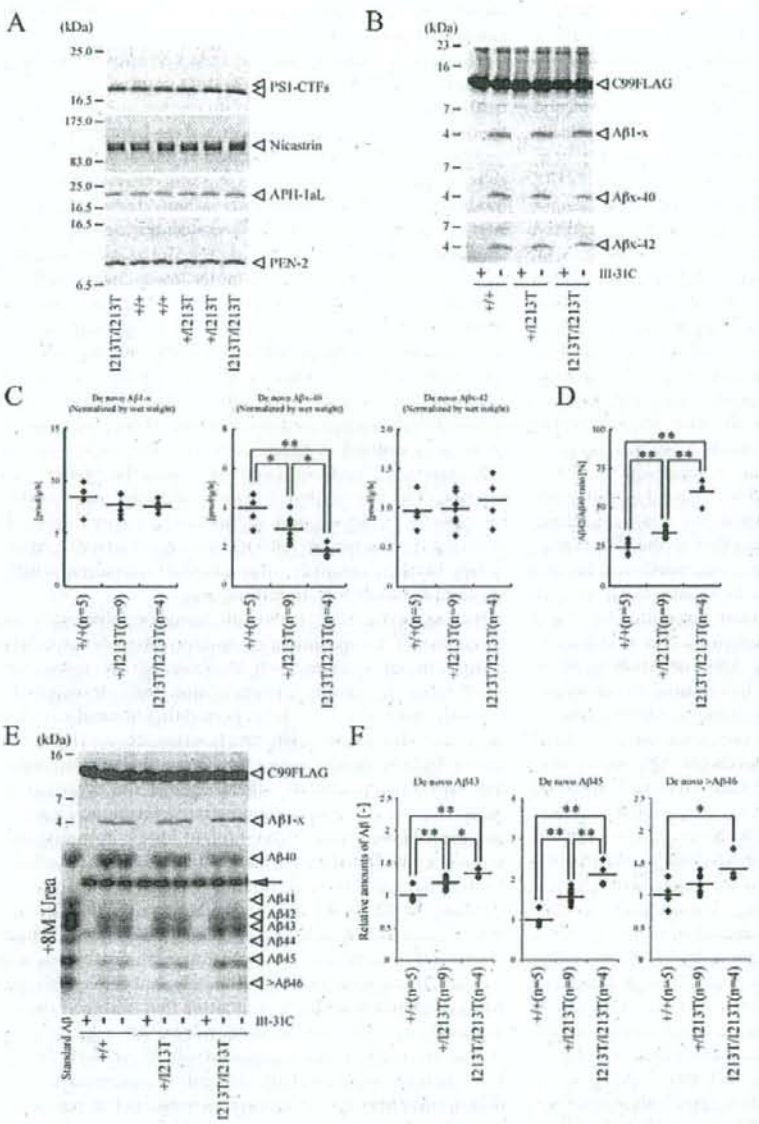

FIGURE 4. **Comparative analysis of γ-secretase activity in I213T knock-in mouse brain.** *A*, the protein levels of each PS complex component were similar in CHAPSO-solubilized microsomal fractions derived from the brains of mice of each genotype. *CTF*, C-terminal fragment. *B*, *de novo* generation of different Aβs was observed in all brain samples, regardless of mouse genotype. Aβ40 signals were significantly reduced in I213T mutant mice. Note that 10 μM WPE-III-31C, a γ-secretase inhibitor, almost completely suppressed Aβ. *C* and *D*, quantitation of the levels of *de novo* generated total Aβ (*C*, *left panel*), Aβ40 (*C*, *middle panel*), and Aβ42 (*C*, *right panel*) in the reaction mixtures is shown. Corresponding Aβ42/Aβ40 ratios are shown in *D*. *Dots* represent the mean values of two independent duplicate experiments ($n = 4$) for each mouse; *horizontal bars* represent the average values of each group. The statistical significance of the data was tested with a Tukey-Kramer test. *, $p < 0.05$; **, $p < 0.01$. *E*, the various Aβ species in the reaction mixtures were separated by SDS-PAGE on 8 M urea-containing Tris-Tricine gels and then probed with 82E1 antibody, The *arrow* indicates carboxyl-truncated C99-FLAG fragments (24). *F*, quantitation of the levels of longer Aβ species is shown. *Dots* represent the mean values of two independent experiments for each mouse; *horizontal bars* represent the average values of each group. The statistical significance of the data was tested with a Tukey-Kramer test. *, $p < 0.05$; **, $p < 0.01$.

we can strictly evaluate the characteristics of native γ-secretase activity without having to consider possible artifacts stemming from overexpression and/or integration of the transgene. To stimulate Aβ generation, we incubated CHAPSO-solubilized fractions containing γ-secretase with 500 nM C99-FLAG for 4 h. We detected *de novo* Aβ synthesis in all samples, regardless of genotype; 10 μM WPE-III-31C inhibitor almost completely blocked γ-secretase activity (Fig. 4*B*). As we observed with the cell models, in I213T PS1 knock-in mice, the I213T mutation significantly reduced Aβ40 levels without obviously affecting Aβ42 levels, leading to higher Aβ42/Aβ40 ratios (Fig. 4, *C* and *D*). The mutant enzyme also increased Aβ43 and Aβ45 levels (Fig. 4, *E* and *F*). Interestingly, the effects of the I213T mutation on γ-secretase activity were much more pronounced in brain samples from homozygous (I213T/I213T) mice than in samples from hemizygous (+/I213T) mice, suggesting that the effect of the I213T mutation is dose-dependent. These findings strongly support the results obtained from the cell models and suggest that FAD mutations directly lead to abnormal alterations in γ-secretase activity, even in the brain under physiological conditions.

DISCUSSION

Although an increased Aβ42/Aβ40 ratio is a common consequence of FAD-linked PS1 mutations, the molecular mechanism underlying this increase still remains controversial (16, 17). Possibly, the increased Aβ42/Aβ40 ratio may result from direct alterations in the cleavage reactions catalyzed by mutant PS/γ-secretase such that Aβ42 generation is facilitated, Aβ40 generation is attenuated, or both Aβ40 and Aβ42 generation change with a different manner. To clarify this crucial issue, we examined the enzymatic characteristics of WT and I213T FAD mutant PS1/γ-secretase in this

study. First, we observed that *de novo* Aβ generation depended on PS protein levels, indicating that our assay system reflects genuine PS-dependent γ-secretase activity. Kinetics analyses revealed that the I213T mutation reduced *de novo* Aβ generation compared with that measured under WT conditions and specifically inhibited the generation of Aβ40 more drastically than of Aβ42. Importantly, these findings were clearly confirmed in experiments of γ-secretase derived from I213T mutant knock-in mouse brains, in which reduction of *de novo* Aβ generation was mutant allele dose-dependent. We reported previously that expression of FAD mutant PS1 in $PS^{-/-}$ MEF cells failed to restore the ability of these cells to secrete Aβ (25). Here, our findings suggest that the reduced secretion levels of Aβ directly correspond to a reduction in the rate of mutant PS1/γ-secretase-mediated cleavage of γ-sites. Taken together, these observations have led us to conclude that the mechanism underlying the increased Aβ42/Aβ40 ratio observed in cases of FAD mutations most likely has to do with the differential reduction of Aβ40 and Aβ42, in which Aβ40 generation is reduced more than Aβ42 generation. Accordingly, the I213T mutation would be expected to lead to a partial loss of γ-site cleavage, which would affect both Aβ40 and Aβ42 generation.

Besides γ-site cleavage at Val^{40} and Ile^{42} of the C terminus, γ-secretase also cleaves APP-CTFβ at two novel sites located closer to the cytoplasmic membrane boundary; these sites are termed ζ-site (Val^{46} of the C terminus) and ε-site (Thr^{48} and Leu^{49} of the C terminus) (18–20). Funamoto *et al.* (34) demonstrated that cell models expressing Aβ49 or Aβ48 prefer to secrete Aβ40 or Aβ42, respectively. In addition, recent studies identified various longer Aβ species (Aβ43 to Aβ49) and demonstrated that DAPT-treated cells contained elevated Aβ43 and Aβ46 levels but reduced Aβ40 levels (21, 22). On the basis of this evidence, it is hypothesized that Aβ40 and Aβ42 are generated as end-products of the γ-secretase-mediated stepwise cleavage of Aβ49 and Aβ48, which occurs at every third residue along the α-helix structure of Aβ49 and Aβ48 after the ε-cleavage site (21, 22). Interestingly, we observed that in cells expressing I213T mutant γ-secretase, *de novo* levels of Aβ43 and >Aβ46 species significantly increased in stages in a C99-FLAG concentration-dependent fashion. If all Aβ species are spontaneously generated from Aβ49/Aβ48 through a one-step reaction after ε-site cleavage, then one would expect the rate of Aβ40, Aβ43, and >Aβ46 generation to demonstrate similar reaction curves because these reactions should have similar K_m values. However, in cells expressing WT PS1 γ-secretase, we clearly observed that only Aβ40 levels reached a plateau at C99-FLAG concentrations over 1.0 μM, whereas Aβ43 and >Aβ46 levels increased linearly in parallel with increasing C99-FLAG concentrations. This finding indicates that each Aβ species is generated from stepwise cleavage (Aβ49 → Aβ46 → Aβ43 → Aβ40) rather than spontaneous cleavage. This would suggest that Aβ43 → Aβ40 might be the rate-limiting step of this reaction pathway. Thus, a reasonable explanation for our results is that the I213T mutation specifically inhibits the γ-site cleavage reaction Aβ43 → Aβ40 and disrupts the kinetic balance of pre-γ-site cleavage reactions (Aβ49 → Aβ46 → Aβ43), leading to higher concentrations of longer Aβ intermediates. Our finding that the Aβ43-generating reaction curve of the I213T mutant enzyme clearly reached a plateau, as did the Aβ40-generating reaction, supports this idea well.

The Aβ42-producing pathway remains controversial. In previous work, Qi-Takahara *et al.* (21) also pointed out that DAPT treatment did not lead to the accumulation of Aβ45 and Aβ48 species, even though it did have a clear inhibitory effect on secreted levels of Aβ42. In the case of PS2/I141I FAD mutant cells, a small accumulation of Aβ45 was observed after DAPT treatment (22). Based on our observations, cleavage reactions of Aβ42 and Aβ45 at C99-FLAG concentrations of >1.5 μM should fit well to stepwise cleavage reactions similar to Aβ48 → Aβ45 → Aβ42. Nevertheless, under lower concentrations of C99-FLAG, we noticed that the I213T mutation constantly facilitated the generation of Aβ45 without affecting Aβ42 levels, suggesting that an additional cleavage pathway that generates Aβ42 may exist. Zhao *et al.* (33) reported recently that Aβ46 may be converted not only to Aβ43 but also to Aβ42, although not through a major pathway. If this were the case, then one reasonable explanation for our observations is that in cells expressing I213T mutant γ-secretase, the Aβ45 → Aβ42 reaction, which is inhibited, may be partially compensated by the Aβ46 → Aβ42 reaction. In this case, a portion of the Aβ42 pool may be a by-product of a miscleavage reaction of Aβ46 → Aβ43. Further detailed enzymological assessments will be required to clarify this important issue.

Increasing the Aβ42/Aβ40 ratio would be sufficient to cause parenchymal Aβ accumulation and formation of toxic Aβ oligomers. In our previous work, we observed that certain Aβ42/Aβ40 ratios accelerate Aβ aggregation and cell toxicity (35). Recently, Kim *et al.* (28) also reported that luminal/extracellular overproduction of Aβ40 clearly attenuates amyloid pathology in Tg2576 mouse brain (36). These observations indicate that Aβ40 has protective effects against the aggregation of Aβ42. As a previous study demonstrated, formic acid-extracted fractions derived from I213T mutant knock-in mouse brains actually contain enhanced levels of Aβ42. Here, we demonstrated that, even though the I213T mutation impaired γ-site cleavage, Aβ42/Aβ40 ratios in the brains of both hemizygous and homozygous knock-in mice remained elevated compared with that in control mice. Thus, in mutant mouse brains, imbalanced Aβ metabolism would ultimately shift the equilibrium of Aβ aggregation potential to a situation that facilitates the accumulation of Aβ42. If this were indeed the case, one would expect the levels of non-aggregated soluble Aβ in the brains of FAD patients to be partially reduced. Recent studies indicate that Aβ may have physiological functions, such as regulation of synaptic plasticity, neuronal survival, or intracellular lipid metabolism (37–40). Thus, the partial lack of functional Aβ species within brain terminals and/or synaptic terminals may also contribute to part of the neurodegenerative process in FAD patients.

Little evidence has been accumulated on longer Aβ species in AD patients and in other Aβ-related abnormal events, and thus it is still unclear whether longer Aβ species contribute to AD pathophysiology. The majority of longer Aβ species are less efficiently secreted and are detected specifically in low density lipid fractions, as they are partially anchored to the membrane (41). Thus, if these membrane-anchored Aβs start to concen-

trate and form abnormal Aβ clusters on low density lipid domains, it is conceivable that these clusters can act as scaffolds to further the formation of toxic Aβ oligomers and/or fibrillar aggregates, which can disrupt membrane fluidity and/or receptor-mediated signaling functions. In this case, the I213T mutation could specifically enhance the steady state levels of longer Aβ species and accelerate abnormal membrane-related Aβ metabolism. Our preliminary results indicate that, like the I213T mutation, some FAD mutations also facilitate the generation of longer Aβ species.[3] Different compositions of different Aβ species may explain the morphological variations in amyloid plaques reported by some immunohistochemical studies of FAD patient brains (42). To understand the overall Aβ-related cascade leading to the onset of AD, continuous effort will be necessary in the near future to elucidate the detailed molecular mechanisms underlying abnormal, FAD-related Aβ metabolism and γ-secretase function.

Acknowledgments—We thank Dr. B. De Strooper for providing $PS^{+/+}$ MEFs and $PS^{-/-}$ MEFs; Dr. A. Murakami-Sekimata (RIKEN Brain Science Institute, Japan) for cDNA constructs encoding human nicastrin, APH-1, and PEN-2; Drs. M. Yoshida and T. Hisabori (Tokyo Institute of Technology, Japan) for helpful discussions; and members of the Laboratory for Alzheimer's Disease for continuous encouragement and support.

REFERENCES

1. Selkoe, D. J. (2001) *Physiol. Rev.* **81**, 741–766
2. Iwatsubo, T., Odaka, A., Suzuki, N., Mizusawa, H., Nukina, N., and Ihara, Y. (1994) *Neuron* **13**, 45–53
3. Iijima, K., Liu, H. P., Chiang, A. S., Hearn, S. A., Konsolaki, M., and Zhong, Y. (2004) *Proc. Natl. Acad. Sci. U. S. A.* **101**, 6623–6628
4. McGowan, E., Pickford, F., Kim, J., Onstead, L., Eriksen, J., Yu, C., Skipper, L., Murphy, M. P., Beard, J., Das, P., Jansen, K., Delucia, M., Lin, W. L., Dolios, G., Wang, R., Eckman, C. B., Dickson, D. W., Hutton, M., Hardy, J., and Golde, T. (2005) *Neuron* **47**, 191–199
5. Borchelt, D. R., Thinakaran, G., Eckman, C. B., Lee, M. K., Davenport, F., Ratovitsky, T., Prada, C. M., Kim, G., Seekins, S., Yager, D., Slunt, H. H., Wang, R., Seeger, M., Levey, A. I., Gandy, S. E., Copeland, N. G., Jenkins, N. A., Price, D. L., Younkin, S. G., and Sisodia, S. S. (1996) *Neuron* **17**, 1005–1013
6. Duff, K., Eckman, C., Zehr, C., Yu, X., Prada, C. M., Perez-tur, J., Hutton, M., Buee, L., Harigaya, Y., Yager, D., Morgan, D., Gordon, M. N., Holcomb, L., Refolo, L., Zenk, B., Hardy, J., and Younkin, S. (1996) *Nature* **383**, 710–713
7. Borchelt, D. R., Ratovitski, T., van Lare, J., Lee, M. K., Gonzales, V., Jenkins, N. A., Copeland, N. G., Price, D. L., and Sisodia, S. S. (1997) *Neuron* **19**, 939–945
8. Bentahir, M., Nyabi, O., Verhamme, J., Tolia, A., Horre, K., Wiltfang, J., Esselmann, H., and De Strooper, B. (2006) *J. Neurochem.* **96**, 732–742
9. Kumar-Singh, S., Theuns, J., Van Broeck, B., Pirici, D., Vennekens, K., Corsmit, E., Cruts, M., Dermaut, B., Wang, R., and Van Broeckhoven, C. (2006) *Hum. Mutat.* **27**, 686–695
10. Selkoe, D. J., and Wolfe, M. S. (2007) *Cell* **131**, 215–221
11. Takasugi, N., Tomita, T., Hayashi, I., Tsuruoka, M., Niimura, M., Takahashi, Y., Thinakaran, G., and Iwatsubo, T. (2003) *Nature* **422**, 438–441
12. Edbauer, D., Winkler, E., Regula, J. T., Pesold, B., Steiner, H., and Haass, C. (2003) *Nat. Cell Biol.* **5**, 486–488
13. Kimberly, W. T., LaVoie, M. J., Ostaszewski, B. L., Ye, W., Wolfe, M. S., and Selkoe, D. J. (2003) *Proc. Natl. Acad. Sci. U. S. A.* **100**, 6382–6387
14. De Strooper, B. (2003) *Neuron* **38**, 9–12
15. Koo, E. H., and Kopan, R. (2004) *Nat. Med.* **10**, (suppl.) S26–S33
16. Wolfe, M. S. (2007) *EMBO Rep.* **8**, 136–140
17. De Strooper, B. (2007) *EMBO Rep.* **8**, 141–146
18. Weidemann, A., Eggert, S., Reinhard, F. B., Vogel, M., Paliga, K., Baier, G., Masters, C. L., Beyreuther, K., and Evin, G. (2002) *Biochemistry* **41**, 2825–2835
19. Gu, Y., Misonou, H., Sato, T., Dohmae, N., Takio, K., and Ihara, Y. (2001) *J. Biol. Chem.* **276**, 35235–35238
20. Zhao, G., Mao, G., Tan, J., Dong, Y., Cui, M. Z., Kim, S. H., and Xu, X. (2004) *J. Biol. Chem.* **279**, 50647–50650
21. Qi-Takahara, Y., Morishima-Kawashima, M., Tanimura, Y., Dolios, G., Hirotani, N., Horikoshi, Y., Kametani, F., Maeda, M., Saido, T. C., Wang, R., and Ihara, Y. (2005) *J. Neurosci.* **25**, 436–445
22. Yagishita, S., Morishima-Kawashima, M., Tanimura, Y., Ishiura, S., and Ihara, Y. (2006) *Biochemistry* **45**, 3952–3960
23. Li, Y. M., Lai, M. T., Xu, M., Huang, Q., DiMuzio-Mower, J., Sardana, M. K., Shi, X. P., Yin, K. C., Shafer, J. A., and Gardell, S. J. (2000) *Proc. Natl. Acad. Sci. U. S. A.* **97**, 6138–6143
24. Kakuda, N., Funamoto, S., Yagishita, S., Takami, M., Osawa, S., Dohmae, N., and Ihara, Y. (2006) *J. Biol. Chem.* **281**, 14776–14786
25. Shimojo, M., Sahara, N., Murayama, M., Ichinose, H., and Takashima, A. (2007) *Neurosci. Res.* **57**, 446–453
26. Herreman, A., Hartmann, D., Annaert, W., Saftig, P., Craessaerts, K., Serneels, L., Umans, L., Schrijvers, V., Checler, F., Vanderstichele, H., Baekelandt, V., Dressel, R., Cupers, P., Huylebroeck, D., Zwijsen, A., Van Leuven, F., and De Strooper, B. (1999) *Proc. Natl. Acad. Sci. U. S. A.* **96**, 11872–11877
27. Herreman, A., Van Gassen, G., Bentahir, M., Nyabi, O., Craessaerts, K., Mueller, U., Annaert, W., and De Strooper, B. (2003) *J. Cell Sci.* **116**, 1127–1136
28. Nakano, Y., Kondoh, G., Kudo, T., Imaizumi, K., Kato, M., Miyazaki, J. I., Tohyama, M., Takeda, J., and Takeda, M. (1999) *Eur. J. Neurosci.* **11**, 2577–2581
29. Tanemura, K., Chui, D. H., Fukuda, T., Murayama, M., Park, J. M., Akagi, T., Tatebayashi, Y., Miyasaka, T., Kimura, T., Hashikawa, T., Nakano, Y., Kudo, T., Takeda, M., and Takashima, A. (2006) *J. Biol. Chem.* **281**, 5037–5041
30. Kimberly, W. T., Esler, W. P., Ye, W., Ostaszewski, B. L., Gao, J., Diehl, T., Selkoe, D. J., and Wolfe, M. S. (2003) *Biochemistry* **42**, 137–144
31. Fraering, P. C., LaVoie, M. J., Ye, W., Ostaszewski, B. L., Kimberly, W. T., Selkoe, D. J., and Wolfe, M. S. (2004) *Biochemistry* **43**, 323–333
32. Yin, Y. I., Bassit, B., Zhu, L., Yang, X., Wang, C., and Li, Y. M. (2007) *J. Biol. Chem.* **282**, 23639–23644
33. Zhao, G., Cui, M. Z., Mao, G., Dong, Y., Tan, J., Sun, L., and Xu, X. (2005) *J. Biol. Chem.* **280**, 37689–37697
34. Funamoto, S., Morishima-Kawashima, M., Tanimura, Y., Hirotani, N., Saido, T. C., and Ihara, Y. (2004) *Biochemistry* **43**, 13532–13540
35. Yoshiike, Y., Chui, D. H., Akagi, T., Tanaka, N., and Takashima, A. (2003) *J. Biol. Chem.* **278**, 23648–23655
36. Kim, J., Onstead, L., Randle, S., Price, R., Smithson, L., Zwizinski, C., Dickson, D. W., Golde, T., and McGowan, E. (2007) *J. Neurosci.* **27**, 627–633
37. Kamenetz, F., Tomita, T., Hsieh, H., Seabrook, G., Borchelt, D., Iwatsubo, T., Sisodia, S., and Malinow, R. (2003) *Neuron* **37**, 925–937
38. Hsieh, H., Boehm, J., Sato, C., Iwatsubo, T., Tomita, T., Sisodia, S., and Malinow, R. (2006) *Neuron* **52**, 831–843
39. Plant, L. D., Boyle, J. P., Smith, I. F., Peers, C., and Pearson, H. A. (2003) *J. Neurosci.* **23**, 5531–5535
40. Grimm, M. O., Grimm, H. S., Patzold, A. J., Zinser, E. G., Halonen, R., Duering, M., Tschape, J. A., De Strooper, B., Muller, U., Shen, J., and Hartmann, T. (2005) *Nat. Cell Biol.* **7**, 1118–1123
41. Yagishita, S., Morishima-Kawashima, M., Ishiura, S., and Ihara, Y. (2008) *J. Biol. Chem.* **283**, 733–738
42. Karlstrom, H., Brooks, W. S., Kwok, J. B., Broe, G. A., Kril, J. J., McCann, H., Halliday, G. M., and Schofield, P. R. (2008) *J. Neurochem.* **104**, 573–583

[3] M. Shimojo, N. Sahara, T. Mizoroki, S. Funamoto, M. Morishima-Kawashima, T. Kudo, M. Takeda, Y. Ihara, H. Ichinose, and A. Takashima, unpublished observations.

European Journal of Pharmacology 592 (2008) 138–145

Contents lists available at ScienceDirect

European Journal of Pharmacology

journal homepage: www.elsevier.com/locate/ejphar

A protective role of unfolded protein response in mouse ischemic acute kidney injury

Worapat Prachasilchai [a,1], Hiroko Sonoda [a,1], Naoko Yokota-Ikeda [b], Sayaka Oshikawa [a], Chie Aikawa [a], Kazuyuki Uchida [c], Katsuaki Ito [a], Takashi Kudo [d], Kazunori Imaizumi [e], Masahiro Ikeda [a,*]

[a] Department of Veterinary Pharmacology, Faculty of Agriculture, University of Miyazaki, Miyazaki, Japan
[b] Nephrology Division, Miyazaki Prefectural Miyazaki Hospital, Miyazaki, Japan
[c] Department of Veterinary Pathology, Faculty of Agriculture, University of Miyazaki, Miyazaki, Japan
[d] Psychiatry, Department of Integrated Medicine, Division of Internal Medicine, Osaka University Graduate School of Medicine, Suita, Japan
[e] Division of Molecular and Cellular Biology, Department of Anatomy, Faculty of Medicine, University of Miyazaki, Miyazaki, Japan

ARTICLE INFO

Article history:
Received 6 March 2008
Received in revised form 3 June 2008
Accepted 27 June 2008
Available online 5 July 2008

Keywords:
Ischemia-reperfusion injury
Endoplasmic reticulum stress
Unfolded protein response
Glucose-regulated protein 78
X-box binding protein
Tunicamycin
Thapsigargin

ABSTRACT

Although renal ischemia-reperfusion is known to activate the unfolded protein response, the renal site and role of activation of this response following the insult *in vivo* remains largely unknown. Here we studied the renal spatio-temporal expression pattern of glucose-regulated protein (GRP) 78, a central regulator of the unfolded protein response network, following renal ischemia-reperfusion and the effects of the specific chemical unfolded protein response inducers, tunicamycin and thapsigargin, on renal ischemia-reperfusion injury in mice. Renal ischemia-reperfusion resulted in expression of the spliced form of the X-box binding protein-1 (XBP-1s) transcript, an unfolded protein response target, at 1 and 2 h after the insult. This response was followed by an increase in the GRP78 transcript and protein. The increased amount of GRP78 protein after ischemia-reperfusion was largely localized in proximal tubule cells. Pretreatment with tunicamycin or thapsigargin significantly ameliorated renal dysfunction and injury after ischemia-reperfusion. Taken together with these results, the unfolded protein response was activated following renal ischemia-reperfusion at sites that are susceptible to ischemia-reperfusion injury, and this activation had a protective effect against renal ischemia-reperfusion injury *in vivo*. Molecules involved in the unfolded protein response may offer new opportunities for pharmacological intervention against renal ischemia-reperfusion injury, which is an important cause of acute kidney injury.

1. Introduction

Ischemia is an important endoplasmic reticulum stress. When protein folding in the endoplasmic reticulum is inhibited by hypoxia, multiple signal transduction pathways that allow cells to respond to hypoxic stress are triggered (Schröder and Kaufman, 2005; Feldman et al., 2005; Xu et al., 2005). These pathways are called the unfolded protein response. The 78-kDa glucose-regulated protein GRP78, also referred to as the immunoglobulin binding protein BiP, belongs to the heat shock protein 70 (HSP70) family (Benjamin and McMillan, 1998) and is a stress-inducible endoplasmic reticulum chaperone that serves as a master modulator for the unfolded protein response network. GRP78 can bind to and inhibit the activation of endoplasmic reticulum stress sensor proteins such as PKR-like endoplasmic reticulum localized kinase (PERK), inositol requiring transmembrane kinase and endonuclease (IRE) 1, and activating transcription factor (ATF) 6. When unfolded proteins accumulate, GRP78 dissociates from the endoplasmic reticulum stress sensor proteins and the unfolded protein response is launched via their activation. PERK is a serine/threonine protein kinase that phosphorylates eukaryotic initiation factor-2α (eIF2α). Phosphorylation of eIF2α inhibits protein translation. IRE1 is an endoribonuclease and kinase, and can excise an intron from the mRNA of X-box binding protein (XBP)-1. The translated protein (XBP-1s) is a basic region/leucine zipper (bZIP) transcription factor that binds to its target sequence in the regulatory regions of chaperone genes to induce their transcription. ATF6, like XBP-1s, is a bZIP transcription factor. After the active form of ATF-6 is produced in response to endoplasmic reticulum stress, it acts as a transcription factor for a range of target genes including endoplasmic reticulum chaperone genes.

Acute kidney injury is a common clinical syndrome characterized by a rapid reduction of the glomerular filtration rate (Lameire et al., 2005; Devarajan, 2006; Xue et al., 2006). Acute kidney injury has been reported in approximately 5% of hospitalized admissions and 30–50% of admissions to intensive care units. The high mortality and morbidity associated with acute kidney injury are related to a lack

* Corresponding author. Department of Veterinary Pharmacology, Faculty of Agriculture, University of Miyazaki, Gakuenkibanadai-nishi 1-1, Miyazaki 889-2192, Japan. Tel./fax: +81 985 58 7268.
E-mail address: a0d302u@cc.miyazaki-u.ac.jp (M. Ikeda).
[1] These authors contributed equally to this work.

0014-2999/$ – see front matter © 2008 Elsevier B.V. All rights reserved.
doi:10.1016/j.ejphar.2008.06.108

of understanding of its underlying molecular mechanisms, and in turn this hampers the development of specific pharmacological interventions (Lameire et al., 2005; Devarajan, 2006; Xue et al., 2006; Ikeda et al., 2006b).

Renal ischemia-reperfusion injury is an important cause of acute kidney injury. As mentioned earlier, the unfolded protein response is activated after hypoxia and therefore the unfolded protein response is thought to have an important role in the pathobiology of ischemia-reperfusion injury. Several studies have indicated that the unfolded protein response is activated after renal ischemia-reperfusion (Kuznetsov et al., 1996; Bando et al., 2004; Montie et al., 2005). However, although GRP78 is known to be a master protein for the unfolded protein response network, the localization and time course of its expression after renal ischemia-reperfusion have not been fully established.

Several specific unfolded protein response inducers, including tunicamycin, thapsigargin, and A23187, have been used in experimental studies of the unfolded protein response (Price and Calderwood, 1992; Kaufman, 1999). Studies of unfolded protein response activation in cultured renal epithelial cells have indicated that it reduces the severity of ischemia-reperfusion-induced cell injury (Bush et al., 1999; George et al., 2004). On the other hand, several *in vivo* studies have shown that treatment with tunicamycin causes apoptosis in renal tubule cells (Zinszner et al., 1998; Nakagawa et al., 2000; Marciniak et al., 2004; Takano et al., 2007). Therefore, the role of unfolded protein response activation in the pathobiology of ischemia-reperfusion injury *in vivo* remains obscure.

In order to obtain insight into the molecular mechanisms underlying renal ischemia-reperfusion injury, and to identify potential therapeutic targets against acute kidney injury, this study investigated the spatio-temporal expression pattern of GRP 78 and the effect of specific chemical unfolded protein response inducers, including tunicamycin and thapsigargin, in a mouse model of renal ischemia-reperfusion injury.

2. Materials and methods

2.1. Animals

All animal studies were in accordance with *Guide for the Care and Use of Laboratory Animals in the University of Miyazaki* and were conducted in compliance with the *Law Concerning the Protection and Control of Animals* (Japanese Law No. 105, October 1, 1973, revised on June 22, 2005), *Standards Relating to the Care and Management of Laboratory Animals and Relief of Pain*, (Notification No.88 of the Ministry of the Environment, Japan, April 28, 2006) and *Guidelines for Animal Experimentation*, (Japanese Association for Laboratory Animal Science, May 22, 1987). Male ddy mice (7 weeks old) were purchased from Kyudo, Inc. (Kumamoto, Japan). The animals were allowed free access to food and water during the study period.

2.2. Renal ischemia-reperfusion and drug administration

The renal ischemia-reperfusion procedure was performed as previously described (Yokota et al., 2002). Briefly, mice weighing 25 to 35 g were anesthetized with pentobarbital (65 to 75 mg/kg) and underwent abdominal incision and dissection of the bilateral renal pedicles. A microvascular clamp (Roboz, MD) was placed on each renal pedicle for 35 min. After the ischemic period, the clamps were removed, the wound was sutured, and the animals were allowed to recover. The animals were kept at constant body temperature with continuous monitoring during the ischemia-reperfusion period, and warmed physiological saline was given just after clamping and before suturing in order to maintain body fluid volume. The total number of animals used for evaluating the time course of renal function (Fig. 1) was 93 (sham, 48; ischemia-reperfusion, 45).

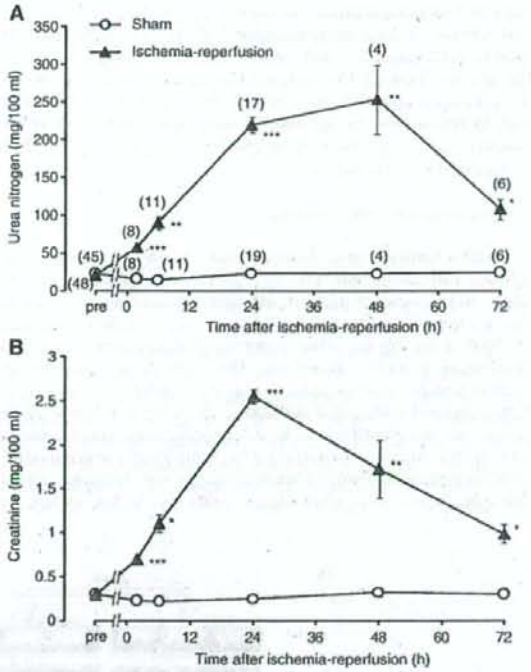

Fig. 1. Renal function after renal ischemia reperfusion. (A, B) Plasma urea nitrogen and creatinine concentrations are shown. Blood was collected more than 48 h before (pre) and 2 h, 6 h, 24 h, 48 h, and 72 h after sham (open circles) or ischemia-reperfusion (closed triangles) operation. Numbers in parentheses are the numbers of animals tested. $^{*}P<0.05$, $^{**}P<0.01$, and $^{***}P<0.001$; significantly different from the value of sham.

Tunicamycin and thapsigargin were purchased from Calbiochem (Darmstadt). Tunicamycin was dissolved in physiological saline and thapsigargin was dissolved in 100% DMSO. Tunicamycin was intraperitoneally administered to mice in a volume of 100 μL/animal 2 days prior to ischemia-reperfusion at a dosage of 1.5 mg/kg. Thapsigarin (1 mg/kg) was administered intraperitoneally to mice in a volume of 100 μL/animal at 24 h prior to ischemia-reperfusion. The control mice were given the corresponding vehicle in the same manner. The above regimen of tunicamycin and thapsigargin administration has been shown to effectively induce the unfolded protein response (Zinszner et al., 1998; Kondoh et al., 2004).

2.3. Renal function evaluation

For chemical analyses, 50-μL blood samples were obtained from the tail blood vessel using a hematocrit capillary, or 1-ml samples were obtained from the inferior vena cava under ether anesthesia at the termination point. Plasma urea nitrogen and creatinine levels were measured with an autoanalyzer (FUJIDRICHEM: Fuji Film Medical Co., Ltd. Tokyo, Japan; TBA-200FR: Toshiba Medical Systems Co., Ltd.,Tokyo, Japan).

2.4. RT-PCR analysis

Total RNA was extracted from whole kidney with the RNeasy® Protect Minikit (Qiagen) with DNase digestion and then cDNA was synthesized from 5 μg of the RNA with the iScript™ cDNA Synthesis kit® (Bio-Rad, CA), according to the respective manufacturer's instructions. Mouse XBP-1, GRP78, and GAPDH mRNA were amplified

with the following primers: forward (5′-gaaccaggagttaagaacacg-3′) and reverse (5′-aggcaacagtgtcagagtcc-3′) for XBP-1, forward (5′-cacgtccaaccccgagaa-3′) and reverse (5′-atgacccgctgatcaaagtc-3′) for GRP78, forward (5′-aacgacccccttcattgac-3′) and reverse (5′-tccacgacatactcagcac-3′) for GAPDH. The number of PCR cycles was 19 for GAPDH, 22 for GRP78, and 35 for XBP-1. All RT-PCR products were analyzed by 1.5% (GRP78 and GAPDH) or 2.5% (XBP-1) agarose gel electrophoresis.

2.5. Preparation of kidney extracts

Mouse kidneys were homogenized in ice-cold homogenate solution containing 300 mM sucrose, 25 mM imidazole, 1.3 mM EDTA, and Complete® protease inhibitor mixture (Roche Molecular Biochemicals, Germany) and the homogenates were then centrifuged at 1000 g for 10 min. The pellet was homogenized again and centrifuged at 1000 g for 10 min. The supernatants from the two centrifugations were combined and the combined solution was subsequently centrifuged at 200,000 g. The pellet from ultracentrifugation was mixed with two volumes of homogenate solution and the protein concentration in a portion of the solution was determined by a DC protein assay kit (Nippon Bio-Rad, Japan). The remaining solution was mixed with 4× Laemmli sample buffer (0.5 M Tris, pH 6.8, 50% glycerol, 8% SDS, 0.05% bromophenolblue) supplemented with 0.2 M dithiothreitol (DTT) and then incubated at 37 °C for 60 min.

2.6. Western blot analysis and chemicals

Western blot analysis was performed as previously reported (Ikeda et al., 2006a). Briefly, after separation by SDS-PAGE, the protein was transferred on to a polyvinylidene difluoride membrane and analyzed by immunoblotting. Antibody-associated protein on the membrane was detected by Super Signal® chemiluminescence detection system (Pierce, IL). Antibodies used in this study were as follows: anti-GRP78 and anti-GAPDH antibodies from Santa Cruz Biotechnology, Inc. (CA), anti-HSP70 antibody from BD Biosciences (CA).

2.7. Histopathological evaluation

For the histopathological evaluation, the left kidney was removed at the indicated time points and fixed in 10% (v/v) neutral buffered formalin. Serial sections of 2 μm thickness were stained with periodic acid-Schiff (PAS). Semi-quantitative analysis was performed by measuring the PAS-positive area. Eight microscope fields were scanned in each mouse by using an image-processing system (Nikon, Tokyo, Japan). For immunohistochemistry, the section was

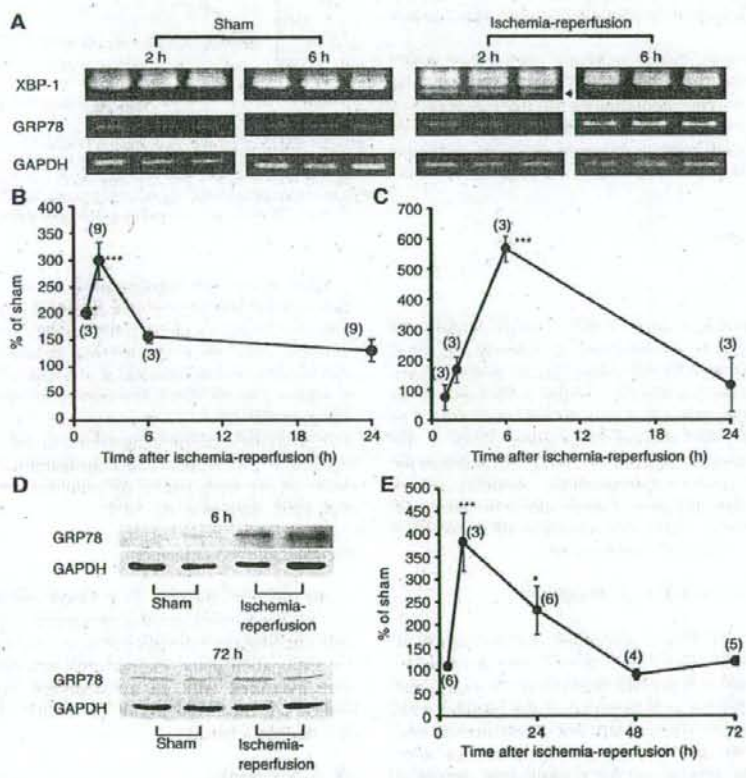

Fig. 2. XBP-1 mRNA, GRP78 mRNA, and GRP78 protein levels after renal ischemia-reperfusion. Mice were subjected to sham or ischemia-reperfusion operation and then total RNA and protein were extracted from whole kidney. (A) A splicing form of XBP-1 mRNA (arrow head) and GRP78 mRNA were determined by RT-PCR with appropriate cycle numbers. GAPDH mRNA was also examined as an internal control. (B, C) Data from the RT-PCR experiments are quantified and summarized for XBP-1s (B) and GRP78 (C) mRNA. Data are expressed as % of the mean value obtained from sham-operated mice, and values represent means ± S. E. M. Numbers in parentheses are the numbers of animals tested. (D) GRP78 and GAPDH (internal control) protein was detected by Western blot. (E) Summarized data from the Western blot experiments. Data are expressed as % of the mean value obtained from sham-operated mice, and values represent means ± S. E. M. Numbers in parentheses are the numbers of animals tested. *$P<0.05$, **$P<0.01$, and ***$P<0.001$; significantly different from the value of sham.

deparaffinized, autoclaved at 121 °C for 5 min, and then immersed into 3% (v/v) H_2O_2 solution diluted in methanol for 10 min at room temperature to block endogenous peroxidase. Thereafter the sections were incubated in a solution containing primary antibody at 37 °C for 60 min followed by incubation with secondary antibodies at 37 °C for 30 min. In order to visualize the protein-antibody complexes, the sections were treated with Envision polymer reagent (DAKO, Tokyo, Japan) at 37 °C for 30 min, followed by treatment with 3,3′-diaminobenzidine tetrahydrochloride. The sections were counter-stained with Mayer's haematoxylin.

2.8. Statistical analysis

Data are expressed as means ± standard error of the mean (S. E. M.). Statistical comparisons among group mean values were performed by Kruskal–Wallis test or ANOVA followed by the Tukey test or Student's *t*-test. Significant difference was accepted at $P<0.05$.

3. Results

3.1. Time course of the change in GRP78 expression after renal ischemia-reperfusion

First, we ascertained a pattern of renal function after ischemia-reperfusion in the mice used in this study. As shown in Fig. 1, plasma urea nitrogen and creatinine concentrations gradually increased, reaching a peak at 48 h after ischemia-reperfusion for urea nitrogen and at 24 h for creatinine, and then decayed.

Next, we examined the time course of expression of the mRNAs for XBP-1s and GRP78, both of which are unfolded protein response targets (Schröder and Kaufman, 2005; Feldman et al., 2005; Xu et al., 2005), using RNA extracted from whole kidney. Fig. 2A shows representative photographs of the RT-PCR experiments and Fig. 2B and C summarize the quantified data. XBP-1s mRNA was clearly up-regulated at 1 h and 2 h after ischemia-reperfusion. This was followed by up-regulation of GRP78 mRNA, which reached a peak at 6 h after ischemia-reperfusion.

We then determined the expression level of GRP78 protein. Protein was extracted from mouse whole kidney and the extracted protein was subjected to immunoblotting. Fig. 2D shows representative blots and Fig. 2E summarizes the quantified data. GRP78 protein was increased at 6 h and 24 h and then decreased to the original level. These data clearly indicate that ischemia-reperfusion activated the unfolded protein response and that this activation preceded the peak of the renal function deficit.

3.2. Distribution of GRP78 in kidney after renal ischemia-reperfusion

The distribution of GRP78 protein was elucidated by immunohistochemistry. As shown in Fig. 3A, slight staining with anti-GRP78 antibody was observed in kidneys from mice subjected to sham operation. In contrast, ischemia-reperfusion produced widespread strong staining with anti-GRP78 antibody in the kidney, especially in the cortico-medullary boundary area (Fig. 3B). At higher magnification (Fig. 3C), the GRP78 protein induced by ischemia-reperfusion could be seen to be mainly distributed in proximal tubular cells. In the proximal tubular cells, GRP78 was located intracellularly.

3.3. Effect of tunicamycin on unfolded protein response targets

Mice were treated with tunicamycin, which is well known to act as an unfolded protein response inducer via inhibition of glycosylation (Price and Calderwood, 1992; Kaufman, 1999), and the expression of unfolded protein response targets was examined. The mice were divided into two groups. The control group was treated with vehicle and the experimental group was treated with 1.5 mg/kg tunicamycin.

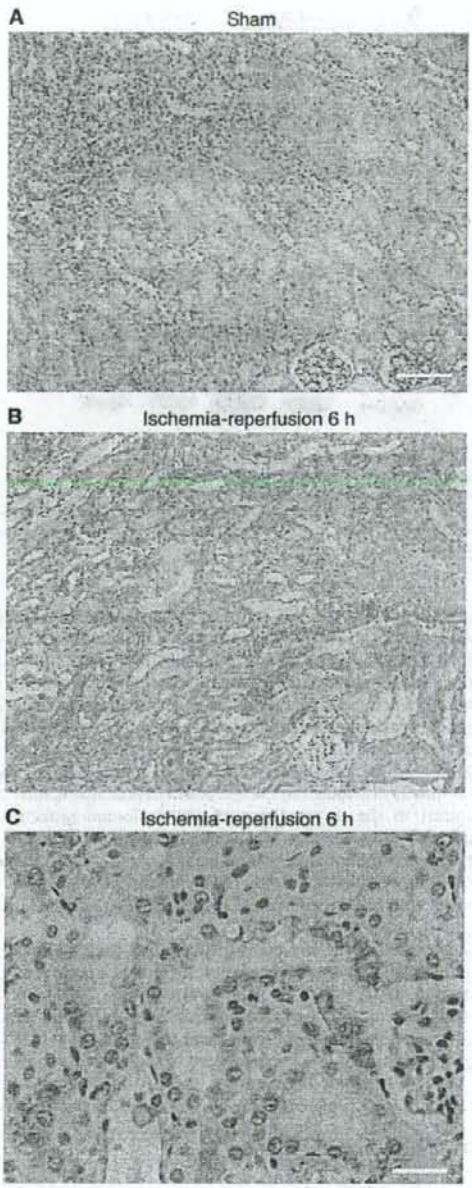

Fig. 3. Immunohistology for GRP78 protein in kidney after renal ischemia-reperfusion. Kidneys were removed 6 h after sham or renal ischemia-reperfusion operation, and were fixed in 10% formaldehyde solution, embedded in paraffin, and then sectioned for immunohistochemical staining with polyclonal rabbit anti-GRP78 antibody. (A) Representative staining in kidney from a mouse subjected to sham operation at low magnification. (B, C) Representative staining in kidney from a mouse subjected to ischemia-reperfusion operation are shown at low (B) and high (C) magnification. Brown staining indicates the presence of GRP78. No brown staining was observed if the primary antibody was omitted (control staining). Scale bars = 100 μm in A and B, 25 μm in C.

Kidney samples were obtained 48 h after the treatments. As shown in Fig. 4A, tunicamycin clearly increased the expression of XBP-1s and GRP78 mRNA. Furthermore, tunicamycin also increased protein

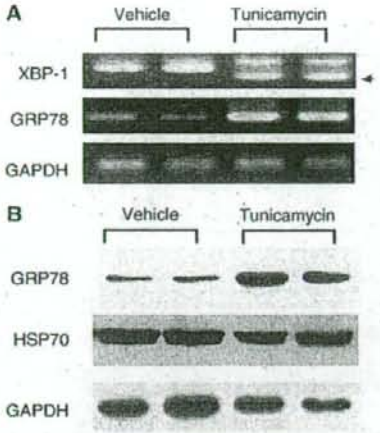

Fig. 4. Effect of treatment with tunicamycin on the expression levels of XBP-1s and GRP78 mRNA, and GRP78 protein. Kidneys were removed 48 h after treatment with vehicle or tunicamycin and then total RNA and protein were extracted. (A) A splicing form of XBP-1 (arrow head), GRP78, and GAPDH mRNA were determined by RT-PCR analysis. (B) GRP78, HSP70 and GAPDH (internal control) protein was detected by Western blot.

expression of GRP78 (Fig. 4B). In contrast, tunicamycin had no effect on the expression level of HSP70, a member of the same protein family as GRP78 (Fig. 4B). Fig. 5 shows the renal distributions of GRP78 after treatment with tunicamycin. Without tunicamycin-treatment, expression of GRP78 was weak (Fig. 5A). After tunicamycin treatment, GRP78 expression markedly increased in the renal cortex and corticomedullary boundary area (Fig. 5B). Higher magnification (Fig. 5C) clearly showed that the GRP78 induced by treatment with tunicamycin was mainly distributed in the cytoplasm of proximal tubular cells. In contrast to the up-regulation of GRP78 immunohistochemical analysis also exhibited that no enhanced expression of HSP70 was observed by treatment with tunicamycin (data not shown), confirming the immunoblotting data. These results clearly show that treatment with tunicamyin specifically induced the unfolded protein response in proximal tubular cells.

We next studied the effect of thapsigargin, which is also known to be an unfolded protein response inducer like tunicamycin (Price and Calderwood, 1992; Kaufman, 1999; Kondoh et al., 2004), on renal GRP78 expression. Kidney samples were obtained 24 h after treatment with thapsigargin. Immunohistochemical analysis showed that thapsigargin up-regulated protein expression of GRP78 in the same renal areas as did tunicamycin (data not shown). In contrast to this, increased expression of HSP70 was not observed by treatment with thapsigargin (data not shown), indicating specific activation of the unfolded protein response by thapsigargin.

3.4. Effect of tunicamycin treatment on ischemia-reperfusion injury

Next, we studied the effect of tunicamycin on renal ischemia-reperfusion injury. Mice were treated with vehicle (control group) or tunicamycin (1.5 mg/kg) 2 days prior to ischemia-reperfusion and kidney samples were obtained 24 h after ischemia-reperfusion. Fig. 6 shows the results of histopathological analysis (PAS staining) and plasma creatinine concentration. Histopathological analysis with PAS staining revealed that ischemia-reperfusion caused cast formation in tubules, tubule dilatation, and epithelial cell death in the cortex and outer medulla (Fig. 6A). Tunicamycin ameliorated these pathological changes (Fig. 6B). Semi-quantitative measurement of the PAS-positive area showed that this was significantly smaller in the tunicamycin group than that in the controls (Fig. 6C). In accordance with the histopathological results, the plasma concentration of creatinine in the tunicamycin group was significantly lower than that in the control group at 24 h after ischemia-reperfusion (Fig. 6D).

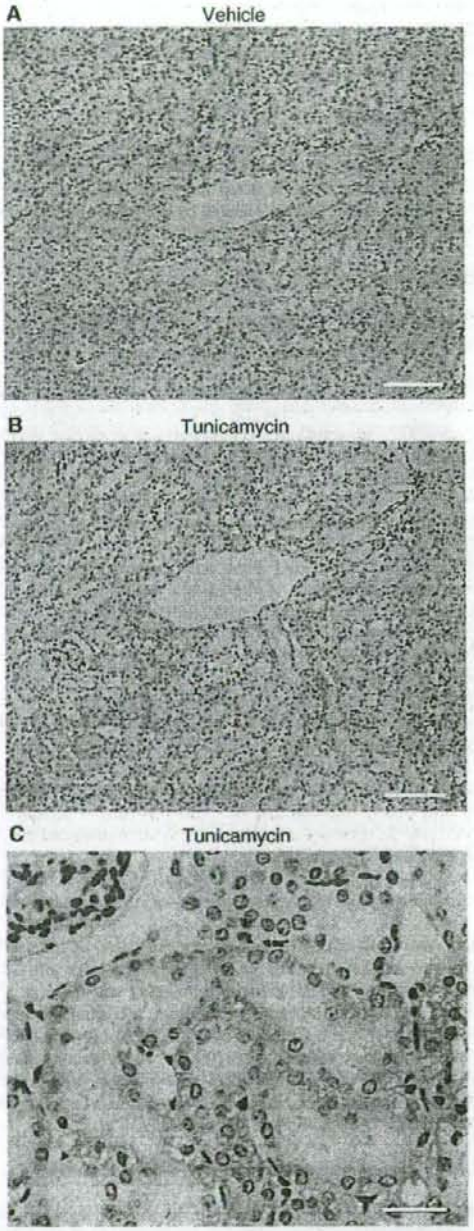

Fig. 5. Immunohistology for GRP78 protein in kidney after treatment with tunicamycin. Kidneys were removed 48 h after treatment with vehicle (PBS) or tunicamycin (1.5 mg/kg). Representative staining for GRP78 protein in kidney after treatment with vehicle at low magnification (A) or with tunicamycin at low (B) and high (C) magnification are shown. Scale bars = 100 μm in A and B, 25 μm in C.

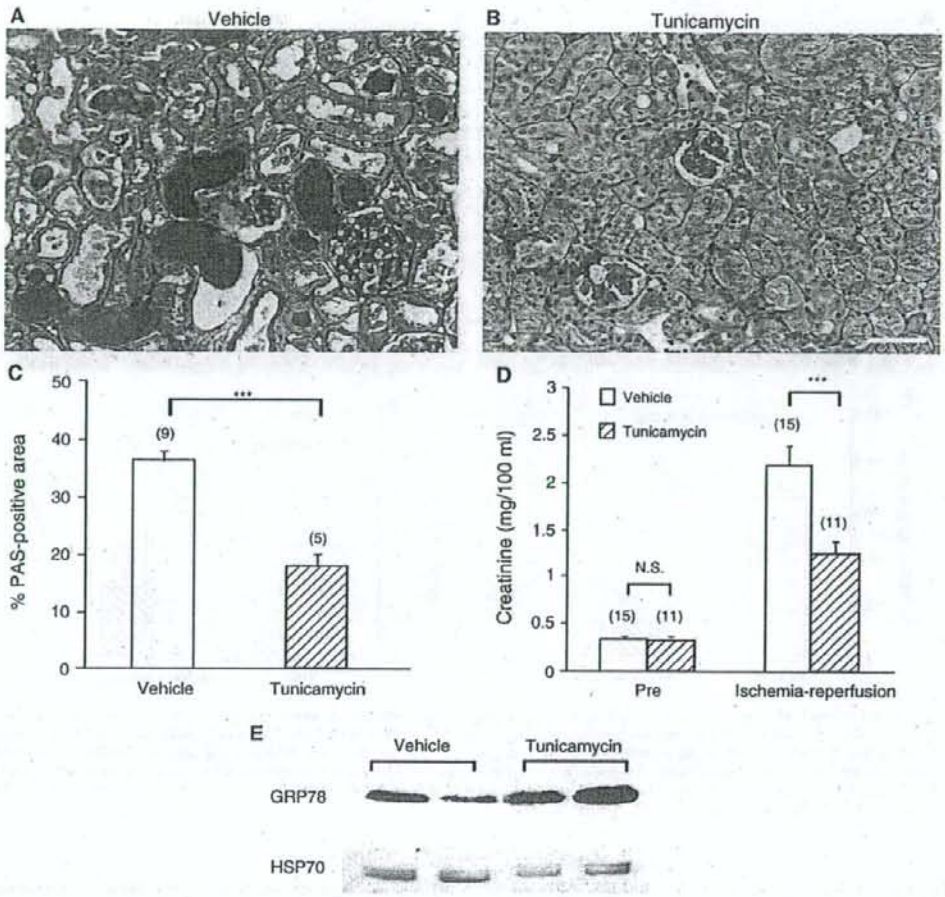

Fig. 6. Effect of tunicamycin on renal ischemia-reperfusion injury. Tunicamycin (1.5 mg/kg) or vehicle (PBS) was administered to mice 48 h before ischemia-reperfusion operation. (A, B, C) PAS staining was performed on kidney sections obtained 24 h after ischemia-reperfusion from mice treated with vehicle (A) or tunicamycin (B). The renal cortex and corticomedullary junction were shown. A scale bar=50 μm. The PAS-positive-area was measured as described in Materials and methods (C). Values are means±S. E. M. Numbers in parentheses are the numbers of animals tested. ***$P<0.001$; significantly different from the value of vehicle-treatment group. (D) Plasma for measurement of creatinine concentration was collected before (Pre) and 24 h after ischemia-reperfusion. Values are means±S. E. M. Numbers in parentheses are the numbers of animals tested. ***$P<0.001$; significantly different from the value of vehicle-treatment group. N.S.; not significantly different from the value of vehicle-treatment group. (E) Representative blots for GRP78 and HSP70. Kidneys treated with vehicle or tunicamysin were removed 24 h after ischemia-reperfusion and protein was extracted.

When we compared the expression level of GRP78 between the control and tunicamycin groups by immunoblotting after renal ischemia-reperfusion, GRP78 expression was clearly higher in the tunicamycin group (Fig. 6E). In contrast, the level of HSP70 expression did not differ between the groups. These data clearly show that treatment of mice with tunicamycin attenuated ischemia-reperfusion injury with concomitant enhancement of renal GRP78 expression.

3.5. Effect of thapsigargin treatment on ischemia-reperfusion injury

Mice were treated with vehicle (control group) or with thapsigargin (1 mg/kg). Fig. 7 shows the results of histopathological analysis and plasma creatinine concentration. Treatment with thapsigargin ameliorated renal function and injury after renal ischemia-reperfusion. As seen in Fig. 7C and D, treatment with the vehicle for thapsigargin (DMSO) tended to reduce the severity of renal injury in comparison with the vehicle for tunicamycin (Fig. 6C and D). Since DMSO is known to be an antioxidant, and reactive oxygen species have been reported to worsen renal ischemia-reperfusion injury, this reduction may be explained by the antioxidant effect of DMSO.

4. Discussion

Several *in vitro* studies with cultured tubular cells have examined the unfolded protein response activation in response to renal ischemia-reperfusion and its role against cell injury using chemical unfolded protein response inducers. In a proteomic study, Kumar et al. (2003) reported that simulated ischemia-reperfusion in cultured tubular LLC-PK1 cells increased GRP78 and HSPs. In Madin–Darby canine kidney cells (Bush et al., 1999; George et al., 2004), ATP depletion by treatment with antimycin, followed by recovery in medium without antimycin, resulted in up-regulation of GRP78. This

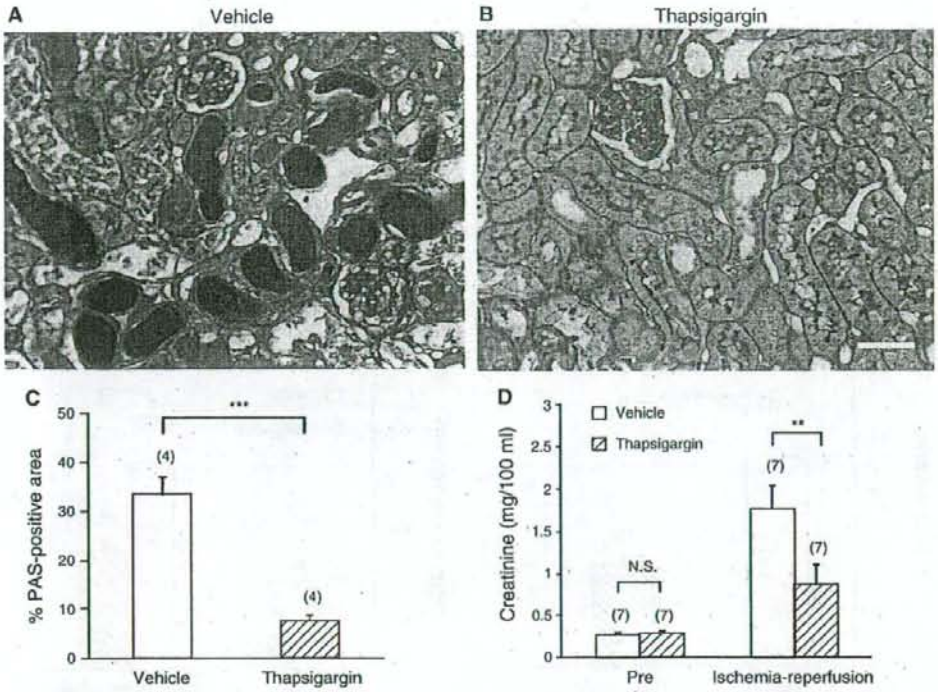

Fig. 7. Effect of thapsigargin on renal ischemia-reperfusion injury. Thapsigargin (1 mg/kg) or vehicle (DMSO) was administered to mice 24 h before ischemia-reperfusion operation. (A, B, C) PAS staining was performed on kidney sections obtained 24 h after ischemia-reperfusion from mice treated with vehicle (A) or thapsigargin (B). The renal cortex and cortico-medullary junction were shown. A scale bar = 50 μm. The PAS-positive-area was measured (C). Values are means ± S. E. M. Numbers in parentheses are the numbers of animals tested. ***$P<0.001$; significantly different from the value of vehicle-treatment group. (D) Plasma for measurement of creatinine concentration was collected before (Pre) and 24 h after ischemia-reperfusion. Values are means ± S. E. M. Numbers in parentheses are the numbers of animals tested. **$P<0.01$; significantly different from the value of vehicle-treatment group. N.S.; not significantly different from the value of vehicle-treatment group.

up-regulation was accompanied by cell injury, and pretreatment of the cells with tunicamycin protected against antimycin-induced cell injury with an enhancement of the expression of GRP78. Nevertheless, although some *in vivo* studies have shown up-regulation of unfolded protein response-related proteins such as GRP78 (Kuznetsov et al., 1996), GRP94 (Kuznetsov et al., 1996), an autophosphorylated form of PERK (Montie et al., 2005), a phosphorylated form of eIF2α (Montie et al., 2005), the 150 kDa oxygen-regulated protein (Bando et al., 2004), and ER protein 72 (Kuznetsov et al., 1996) in mouse kidney after ischemia-reperfusion, the role of activation of the unfolded protein response in renal ischemia-reperfusion injury *in vivo* remains largely unknown. In the present study, we clearly showed that ischemia-reperfusion caused up-regulation of GRP78. This GRP78 was mainly distributed in the cortico-medullary boundary area, especially in the interior of proximal tubular cells, which is known to be susceptible to renal ischemia-reperfusion injury. Up-regulation of the chemical unfolded protein response was apparent at 6 h after ischemia-reperfusion, and this response subsequently returned to its original level within 24 h. Treatement with tunicamycin, known to be a specific chemical unfolded protein response inducer, clearly induced GRP78 expression mainly in the cortico-medullary boundary area. Pretreatment of mice with tunicamycin protected tubule cells from renal ischemia-reperfusion injury with enhancement of GRP78 protein expression. Thapsigargin, another inducer of chemical unfolded protein response, mimicked the effect of tunicamycin. Taken together with the earlier *in vitro* data, these observations provide strong evidence that the unfolded protein response is activated in the renal sites that are susceptible to ischemia-reperfusion injury, and that this activation is involved in protection against this type of injury. To our knowledge, this is the first study to have demonstrated a protective effect of chemical unfolded protein response inducers against renal ischemia-reperfusion injury *in vivo*.

We observed strong expression of GRP78 at the cortico medullary junction in response to ischemia-reperfusion. A phosphorylated form of eIF2α has been reported to be localized in the same region after renal ischemia-reperfusion (Montie et al., 2005). These data indicate that activation of the unfolded protein response occurs predominantly in this region, which is known to be poorly vascularized (Montie et al., 2005) and susceptible to renal ischemia-reperfusion. In addition, Yin et al. (2002) observed a dramatic increase of hypoxia at the cortico-medullary junction 24 h after renal ischemia-reperfusion relative to that in the cortex and inner medulla. Therefore, the selective induction of GRP78 in this area may be a reflection of the severity of hypoxia following ischemia-reperfusion.

Administration of tunicamycin to mice causes renal tubular cell apoptosis through activation of the unfolded protein response. Ron and colleagues examined the role of the C/EBP homologous protein-10 (CHOP), also known as GADD153, which is a molecule downstream from PERK, in *chop* −/− mice treated with tunicamycin (Zinszner et al., 1998; Marciniak et al., 2004). They showed that tunicamycin induced conspicuous renal tubule cell apoptosis in the juxtamedullary region of wild-type mice and that this apoptosis was reduced in *chop* −/− mice, suggesting that tunicamycin-induced renal epithelial apoptosis is partly mediated by the PERK-CHOP pathway. Using mice, Nakagawa

et al. (2000) studied the involvement of caspase-12, an endoplasmic reticulum stress-related, in renal tubule epithelial cell death after tunicamycin treatment. Wild-type mice injected with tunicamycin showed a significant number of TUNEL-positive (DNA-fragmented) renal epithelial cells, whereas fewer TUNEL-positive cells were found in *caspase-12* −/− kidney. This also suggests that tunicamycin causes epithelial cell apoptosis via activation of the unfolded protein response and therefore that treatment with tunicamycin alone might cause renal injury. However, in the present study treatment with tunicamycin alone had no effect on renal function (Fig. 6D), and moreover had a protective effect against renal ischemia-reperfusion injury. Similar findings have also been obtained by several other groups (Zinszner et al., 1998; Takano et al., 2007). It is currently unclear why tunicamycin can either ameliorate renal ischemia-reperfusion injury or cause apoptosis, but one possible explanation is a dual effect of unfolded protein response activation, which may lead to differential susceptibility of tubule epithelial cells via either a pro-survival or a pro-apoptotic phenotype. A minor population of renal tubule epithelial cells subjected to more intense unfolded protein response activation by tunicamycin might undergo apoptotic cell death, whereas a larger number of less intensely affected renal tubule cells might suffer inhibition of protein synthesis that is caused by unfolded protein response activation, which is followed by an increase in the processing capacity of the endoplasmic reticulum, leading to cell recovery from ischemia-reperfusion injury.

HSP70 belongs to the same protein family as GRP78 (Benjamin and McMillan, 1998). It has been reported that HSP70 is up-regulated by ischemia-reperfusion and that this up-regulation leads to protection against renal ischemia-reperfusion injury (Suzuki et al., 2005). We therefore examined whether HSP70 was involved in protection by chemical unfolded protein response inducers against renal ischemia-reperfusion injury. None of the inducers such as tunicamycin and thapsigargin affected the expression of HSP70, suggesting that the unfolded protein response inducers used in this study exerted their effects independently of HSP70. Furthermore, we determined the expression level of HSC70, which is also a member of the HSP70 protein family (Benjamin and McMillan, 1998), and again found that expression of HSC70 was not affected by chemical unfolded protein response inducers (data not shown). These observations support the specificity of the chemical unfolded protein response inducers used in this study.

In the response to ischemia-reperfusion, up-regulation of XBP-1s transcript clearly preceded that of GRP78 transcript. Since transactivation of the gene by XBP-1s has been shown to be dependent on a sequence present in the GRP78 promoter, this strongly suggests that XBP-1s functions as a transcription factor for GRP78. In fact, the level of GRP78 mRNA has been reported to be constitutively elevated in cells overproducing XBP-1 (Yoshida et al., 2001). However, Lee et al. (2003) showed that the induction of GRP78 by tunicamycin was only modestly dependent on XBP-1 in XBP-1-deficient mouse embryo fibroblast cells as well as in XBP-1/ATF6α doubly deficient mouse embryo fibroblast cells, and they concluded that there is an additional *cis*-acting element in addition to those for XBP-1s and ATF6 in the GRP78 promoter that is responsible for its endoplasmic reticulum-stress-induced expression. In contrast to this report, Thuerauf et al. (2006) recently investigated the functional role of XBP-1 in cultured cardiac myocytes infected with a recombinant adenovirus encoding dominant-negative XBP-1 and then subjected to tunicamycin and hypoxia/reoxygenation. They observed that GRP78 expression in response to treatment with tunicamycin and to hypoxia/reoxygenation depended on the expression level of XBP-1, and that expression of dominant-negative XBP-1 worsened hypoxia/reoxygenation-induced cell injury. Together, these reports suggest a cell-type-dependence for the regulation of GRP78 expression by XBP-1. The detailed molecular mechanisms by which renal ischemia-reperfusion up-regulates GRP78 await clarification in future studies.

Acknowledgements

This work was supported in part by JSPS KAKENHI, 19580342 (M.I.).

References

Bando, Y., Tsukamoto, Y., Katayama, T., Ozawa, K., Kitao, Y., Hori, O., Stern, D.M., Yamauchi, A., Ogawa, S., 2004. ORP150/HSP12A protects renal tubular epithelium from ischemia-induced cell death. FASEB J. 18, 1401–1403.

Benjamin, I.J., McMillan, D.R., 1998. Stress (heat shock) proteins: molecular chaperones in cardiovascular biology and disease. Circ. Res. 83, 117–132.

Bush, K.T., George, S.K., Zhang, P.L., Nigam, S.K., 1999. Pretreatment with inducers of ER molecular chaperones protects epithelial cells subjected to ATP depletion. Am. J. Physiol. Renal Physiol. 277, F211–F218.

Devarajan, P., 2006. Update on mechanisms of ischemic acute kidney injury. J. Am. Soc. Nephrol. 17, 1503–1520.

Feldman, D.E., Chauhan, V., Koong, A.C., 2005. The unfolded protein response: a novel component of the hypoxic stress response in tumors. Mol. Cancer Res. 3, 597–605.

George, S.K., Meyer, T.N., Abdeen, O., Bush, K.T., Nigam, S.K., 2004. Tunicamycin preserves intercellular junctions, cytoarchitecture, and cell-substratum interactions in ATP-depleted epithelial cells. Biochem. Biophys. Res. Commun. 322, 223–231.

Ikeda, M., Gunji, Y., Sonoda, H., Oshikawa, S., Shimono, M., Horie, A., Ito, K., Yamasaki, S., 2006a. Shiga toxin activates p38 MAP kinase through cellular Ca(2+) increase in Vero cells. Eur. J. Pharmacol. 546, 36–39.

Ikeda, M., Prachasilchai, W., Burne-Taney, M.J., Rabb, H., Yokota-Ikeda, N., 2006b. Ischemic acute tubular necrosis models and drug discovery: a focus on cellular inflammation. Drug Discov. Today 11, 364–370.

Kaufman, R.J., 1999. Stress signaling from the lumen of the endoplasmic reticulum: coordination of gene transcriptional and translational controls. Genes Dev. 13, 1211–1233.

Kondoh, M., Tsukada, M., Kuronaga, M., Higashimoto, M., Takiguchi, M., Himeno, S., Watanabe, Y., Sato, M., 2004. Induction of hepatic metallothionein synthesis by endoplasmic reticulum stress in mice. Toxicol. Lett. 148, 133–139.

Kumar, Y., Tatu, U., 2003. Stress protein flux during recovery from simulated ischemia: induced heat shock protein 70 confers cytoprotection by suppressing JNK activation and inhibiting apoptotic cell death. Proteomics 3, 513–526.

Kuznetsov, G., Bush, K.T., Zhang, P.L., Nigam, S.K., 1996. Perturbations in maturation of secretory proteins and their association with endoplasmic reticulum chaperones in a cell culture model for epithelial ischemia. Proc. Natl. Acad. Sci. U. S. A. 93, 8584–8589.

Lameire, N., Van Biesen, W., Vanholder, R., 2005. Acute renal failure. Lancet 365, 417–430.

Lee, A.H., Iwakoshi, N.N., Glimcher, L.H., 2003. XBP-1 regulates a subset of endoplasmic reticulum resident chaperone genes in the unfolded protein response. Mol. Cell. Biol. 23, 7448–7459.

Marciniak, S.J., Yun, C.Y., Oyadomari, S., Novoa, I., Zhang, Y., Jungreis, R., Nagata, K., Harding, H.P., Ron, D., 2004. CHOP induces death by promoting protein synthesis and oxidation in the stressed endoplasmic reticulum. Genes Dev. 18, 3066–3077.

Montie, H.L., Kayali, F., Haezebrouck, A.J., Rossi, N.F., Degracia, D.J., 2005. Renal ischemia and reperfusion activates the eIF 2 alpha kinase PERK. Biochim. Biophys. Acta 1741, 314–324.

Nakagawa, T., Zhu, H., Morishima, N., Li, E., Xu, J., Yankner, B.A., Yuan, J., 2000. Caspase-12 mediates endoplasmic-reticulum-specific apoptosis and cytotoxicity by amyloid-beta. Nature 403, 98–103.

Price, B.D., Calderwood, S.K., 1992. Gadd45 and Gadd153 messenger RNA levels are increased during hypoxia and after exposure of cells to agents which elevate the levels of the glucose-regulated proteins. Cancer Res. 52, 3814–3817.

Schröder, M., Kaufman, R.J., 2005. The mammalian unfolded protein response. Annu. Rev. Biochem. 74, 739–789.

Suzuki, S., Maruyama, S., Sato, W., Morita, Y., Sato, F., Miki, Y., Kato, S., Katsuno, M., Sobue, G., Yuzawa, Y., Matsuo, S., 2005. Geranylgeranylacetone ameliorates ischemic acute renal failure via induction of Hsp70. Kidney Int. 67, 2210–2220.

Takano, K., Tabata, Y., Kitao, Y., Murakami, R., Suzuki, H., Yamada, M., Iinuma, M., Yoneda, Y., Ogawa, S., Hori, O., 2007. Methoxyflavones protect cells against endoplasmic reticulum stress and neurotoxin. Am. J. Physiol., Cell Physiol. 292, C353–C361.

Thuerauf, D.J., Marcinko, M., Gude, N., Rubio, M., Sussman, M.A., Glembotski, C.C., 2006. Activation of the unfolded protein response in infarcted mouse heart and hypoxic cultured cardiac myocytes. Circ. Res. 99, 275–282.

Xu, C., Bailly-Maitre, B., Reed, J.C., 2005. Endoplasmic reticulum stress: cell life and death decisions. J. Clin. Invest. 115, 2656–2664.

Xue, J.L., Daniels, F., Star, R.A., Kimmel, P.L., Eggers, P.W., Molitoris, B.A., Himmelfarb, J., Collins, A.J., 2006. Incidence and mortality of acute renal failure in medicare beneficiaries, 1992 to 2001. J. Am. Soc. Nephrol. 17, 1135–1142.

Yin, M., Zhong, Z., Connor, H.D., 2002. Protective effect of glycine on renal injury induced by ischemia-reperfusion in vivo. Am. J. Physiol. Renal Physiol. 282, F417–F423.

Yokota, N., Daniels, F., Crosson, J., Rabb, H., 2002. Protective effect of T cell depletion in murine renal ischemia-reperfusion injury. Transplantation 74, 759–763.

Yoshida, H., Matsui, T., Yamamoto, A., Okada, T., Mori, K., 2001. XBP1 mRNA is induced by ATF6 and spliced by IRE1 in response to ER stress to produce a highly active transcription factor. Cell 107, 881–891.

Zinszner, H., Kuroda, M., Wang, X., Batchvarova, N., Lightfoot, R.T., Remotti, H., Stevens, J.L., Ron, D., 1998. CHOP is implicated in programmed cell death in response to impaired function of the endoplasmic reticulum. Genes Dev. 12, 982–995.

Journal of Neurochemistry

JOURNAL OF NEUROCHEMISTRY | 2008 | 107 | 279–290

doi: 10.1111/j.1471-4159.2008.05606.x

Reduced retinal function in amyloid precursor protein-overexpressing transgenic mice via attenuating glutamate-*N*-methyl-D-aspartate receptor signaling

Masamitsu Shimazawa,* Yuta Inokuchi,* Takashi Okuno,† Yoshihiro Nakajima,‡ Gaku Sakaguchi,‡ Akira Kato,‡ Hidehiro Oku,† Tetsuya Sugiyama,† Takashi Kudo,§ Tsunehiko Ikeda,† Masatoshi Takeda§ and Hideaki Hara*

**Department of Biofunctional Evaluation, Laboratory of Molecular Pharmacology, Gifu Pharmaceutical University, Gifu, Japan*

†Department of Ophthalmology, Osaka Medical College, Takatsuki, Japan

‡Discovery Research Laboratories, Shionogi and Co. Ltd., Shiga, Japan

§Department of Psychiatry, Osaka University Graduate School of Medicine, Osaka, Japan

Abstract

Here, we examined whether amyloid-β (Aβ) protein participates in cell death and retinal function using three types of transgenic (Tg) mice *in vivo* [human mutant amyloid precursor protein (APP) Tg (Tg 2576) mice, mutant presenilin-1 (PS-1) knock-in mice, and APP/PS-1 double Tg mice]. ELISA revealed that the insoluble form of $A\beta_{1-40}$ was markedly accumulated in the retinas of APP and APP/PS-1, but not PS-1 Tg, mice (vs. wild-type mice). In APP Tg and APP/PS-1 Tg mice, immunostaining revealed accumulations of intracellular $A\beta_{1-42}$ in retinal ganglion cells and in the inner and outer nuclear layers. APP Tg and APP/PS-1 Tg, but not PS-1 Tg, mice had less NMDA-induced retinal damage than wild-type mice, and the reduced damage in APP/PS-1 Tg mice was diminished by the pre-treatment of *N*-[*N*-(3,5-difluorophenacetyl)-L-alanyl]-*S*-phenylglycine t-butyl ester, a γ-secretase inhibitor. Furthermore, the number of TUNEL-positive cells was significantly less in ganglion cell layer of APP/PS-1 Tg mice than PS-1 Tg mice 24 h after NMDA injection. The phosphorylated form of calcium/calmodulin-dependent protein kinase IIα (CaMKIIα), but not total CaMKIIα or total NMDA receptor 1 (NR1) subunit, in total retinal extracts was decreased in non-treated retinas of APP/PS-1 Tg mice (vs. wild-type mice). CaMKIIα and NR2B proteins, but not NR1, in retinal membrane fraction were significantly decreased in APP/PS-1 Tg mice as compared with wild-type mice. The NMDA-induced increase in p-CaMKIIα in the retina was also lower in APP/PS-1 Tg mice than in wild-type mice. In electroretinogram and visual-evoked potential recordings, the implicit time to each peak from a light stimulus was prolonged in APP/PS-1 mice versus wild-type mice. Hence, Aβ may impair retinal function by reducing activation of NMDA-receptor signaling pathways.

Keywords: amyloid-β, electroretinogram, *N*-methyl-D-aspartate, retinal ganglion cell death, transgenic mice, visual-evoked potential.

J. Neurochem. (2008) **107**, 279–290.

Alzheimer's disease (AD) is characterized by the accumulation of amyloid β peptide (Aβ) within the brain. Aβ is constitutively produced by proteolysis of β-amyloid precursor protein (APP). Since the pathological formation of amyloid plaques is thought to be the primary force driving the pathogenesis of Alzheimer's disease, much attention has been focused on the production of Aβ. With regard to retinal diseases, it has been demonstrated that Aβ deposition is also increased in patients with age-related macular degeneration – in this case within drusen, rather than within the brain – and that Aβ assemblies are most prevalent in eyes in which drusen is present (Johnson *et al.* 2002; Dentchev *et al.*

Received June 12, 2008; revised manuscript received July 16, 2008; accepted July 28, 2008.

Address correspondence and reprint requests to Professor H. Hara, PhD, Department of Biofunctional Evaluation, Laboratory of Molecular Pharmacology, Gifu Pharmaceutical University, 5-6-1 Mitahora-higashi, Gifu 502-8585, Japan. E-mail: hidehara@gifu-pu.ac.jp

Abbreviations used: APP, amyloid precursor protein; DAPT, *N*-[*N*-(3,5-difluorophenacetyl)-L-alanyl]-*S*-phenylglycine t-butyl ester; DEA, diethylamine; ERG, electroretinogram; GCL, ganglion cell layer; IPL, inner plexiform layer; PBS, phosphate-buffered saline; RGC, retinal ganglion cells; VEP, visual-evoked potential.

2003). On the basis of these findings, Aβ deposition within drusen could be either a cause or a consequence of the degeneration of retinal pigment epithelium and/or photoreceptors in age-related macular degeneration.

A few years ago, Bayer *et al.* (2002) noted that Alzheimer's patients had a greater rate of glaucoma occurrence (25.9%) than a control group (5.2%). Subsequently, we reported (i) that the concentrations of $A\beta_{42}$ and tau were decreased and increased, respectively, in vitreous fluid from patients with glaucoma and diabetic retinopathy (vs. macular hole controls), (ii) that in proliferative diabetic retinopathy patients, there was a significant increase in the activity of neprilysin, a rate-limiting peptidase involved in the physiological degradation of Aβ, and (iii) that β-secretase inhibitors reduced glutamate-induced cell death in rat primary cultured retinal ganglion cells (Yamamoto *et al.* 2004; Yoneda *et al.* 2005; Hara *et al.* 2006).

Glaucoma, one of the leading causes of blindness, is an optic neuropathy characterized by RGC death. Actually, RGC death is a common feature of many ophthalmic disorders, such as glaucoma, optic neuropathies, and various retinovascular diseases (diabetic retinopathy and retinal vein occlusions). RGC death has been reported to occur via a variety of mechanisms involving, for example, oxidative stress (Bonne *et al.* 1998), excitatory amino acids (Dreyer 1998), and nitric oxide (NO) (Neufeld 1999). Glaucoma in humans is associated with a significant elevation in the vitreal glutamate concentration (Dreyer *et al.* 1996). This is important since in the retina, RGC are exquisitely sensitive to the effects of glutamate and its analog *N*-methyl-D-aspartate (NMDA), which produces cell loss both *in vivo* and *in vitro*, and since glutamate toxicity has been implicated in the pathophysiology of glaucoma (as it has in Alzheimer's disease) (Dreyer 1998; Harkany *et al.* 2000). Interestingly, McKinnon *et al.* (2002) found that a chronic elevation of intraocular pressure (IOP) induces Aβ production in RGC and reduces the amounts of full-length APP in rat retinas. Furthermore, Guo *et al.* (2007) have reported that a neutralizing antibody to Aβ significantly delays and attenuates RGC apoptosis in experimental glaucoma. These findings indicate a possible causal role for Aβ in the pathophysiology of retinal disorders, although little is known about participation in RGC death or retinal function. Here, we aimed to examine whether Aβ participates in RGC death, retinal function, or visual function. For this, we employed three murine models of Alzheimer's disease *in vivo* [namely, human mutant APP Tg (Tg 2576) mice, mutant presenilin-1 (PS-1) knock-in, mice and APP/PS-1 double Tg mice].

Materials and methods

Animals

Three types of transgenic (Tg) mice and littermate wild-type mice on a B6SJLF1 background (adult males aged between 11 and 24 months) were used in this study: human mutant APP Tg (Tg 2576) mice (Taconic, Hudson, NY, USA), mutant presenilin-1 (PS-1) knock-in mice generated by Nakano *et al.* (1999), and APP/PS-1 double Tg mice. The APP Tg mouse (Tg2576) carries a transgene (coding for the 695 amino acid isoform of human APP) derived from a large Swedish family with early-onset Alzheimer's disease (Hsiao *et al.* 1996). The PS-1 knock-in mouse carries a transgene derived from a Japanese family with familial Alzheimer's disease caused by the I213T mutation of PS-1 (Nakano *et al.* 1999). The APP/PS-1 double Tg mouse was generated by cross-breeding these two lines.

Retinal injury

Retinal damage was induced by intravitreal injection (2 μL/eye) of NMDA (Sigma-Aldrich, St. Louis, MO, USA) dissolved at 2.5 mM in 0.01 mol/L phosphate-buffered saline (PBS) under isoflurane anesthesia as described in our previous report (Shimazawa *et al.* 2007b). A γ-secretase inhibitor, *N*-[*N*-(3,5-difluorophenacetyl)-L-alanyl]-*S*-phenylglycine t-butyl ester (DAPT, Sigma–Aldrich) was dissolved in corn oil containing 10% ethanol, and DAPT (100 mg/kg) or vehicle (10 mL/kg) was subcutaneously administered to PS-1 knock-in and APP/PS-1 Tg mice 3 h before and just after the intravitreal injection of NMDA.

Histological analysis

Seven days after the NMDA injection, eyeballs were enucleated, prepared retinal-cross sections stained with hematoxylin and eosin, and retinal damage was evaluated as described in our previous report (Shimazawa *et al.* 2007a).

ELISA in retina

To measure soluble or insoluble $A\beta_{1-40}$, mouse retinas were homogenized in diethylamine (DEA) solution (0.2% DEA and 50 mM NaCl), then centrifuged at 100 000 *g* for 60 min. The supernatants were used as the soluble fraction, while the pellets [dissolved in guanidine hydrochloride (Gu-HCl) solution (5 mol/L Gu-HCl in 50 mmol/L Tris-buffered saline, pH 8)] were used as the insoluble fraction. The concentration of $A\beta_{1-40}$ in those fractions of retina was measured using a high-sensitivity human $A\beta_{1-40}$ ELISA assay kit (Immuno-Biological Laboratories Co., Ltd., Takasaki, Japan), because retinal sample needed higher sensitivity to detect $A\beta_{1-40}$ than brain (see Appendix S1 in Supporting information).

Membrane extracts of retina

The membrane fraction rich in integral membranes and membrane-associated proteins was isolated in accordance with the protocol provided for a commercially available ProteoExtract™ Native Membrane Protein Extraction Kit (M-PEK, Cat. No. 444810; Calbiochem, San Diego, CA, USA; http://www.emdbiosciences.com/docs/docs/PROT/444810.pdf).

Immunoblotting

Mouse retinas were lysed using a cell-lysis buffer [RIPA buffer (R0278; Sigma–Aldrich) with protease (P8340; Sigma–Aldrich) and phosphatase inhibitor cocktails (P2850 and P5726; Sigma–Aldrich), and 1 mM EDTA]. Cell lysates or membrane extracts were solubilized in sodium dodecyl sulfate-sample buffer, separated on 10% sodium dodecyl sulfate-polyacrylamide gels, and transferred to

